Nova proteins direct synaptic integration of somatostatin interneurons through activity-dependent alternative splicing

Brie Wamsley[1,3,7+], Leena A. Ibrahim[3,4,7], Nusrath Yusuf[1,3,4], Elaine Fisher[3,4], Xavier Hubert Jaglin[1,3], Qing Xu[5], Lihua Guo[5], Alireza Khodadadi-Jamayran[2], Emilia Favuzzi[3,4], Yuan Yuan[6], Jordane Dimidschstein[4], Robert Darnell[6], and Gord Fishell[1,3,4,#]

[1] NYU Neuroscience Institute and the Department of Neuroscience and Physiology; Smilow Research Center, New York University School of Medicine, 522 First Avenue; New York, NY 10016, USA.
[2] Genome Technology Center, Applied Bioinformatics Laboratories, NYU Langone Medical Center; 550 First Avenue, MSB 304; New York, NY 10016, USA.
[3]Department of Neurobiology, Harvard Medical School, 220 Longwood Ave., Boston, MA 02115
[4]Stanley Center at the Broad, 75 Ames St., Cambridge, MA 02142
[5]Center for Genomics & Systems Biology, New York University, Abu Dhabi, UAE
[6]Laboratory of Molecular Neuro-Oncology, The Rockefeller University, New York, NY
[7] These authors contributed equally
+Current address: Department of Neurology, David Geffen School of Medicine, UCLA, Los Angeles, CA, USA
[#] Lead and corresponding author: gordon_fishell@hms.harvard.edu

Abstract

Somatostatin interneurons are the earliest born population of inhibitory cells. They are crucial to support normal brain development and function; however, the mechanisms underlying their integration into nascent cortical circuitry are not well understood. In this study, we begin by demonstrating that the maturation of somatostatin interneurons is activity dependent. We then investigated the relationship between activity, alternative splicing and synapse formation within this population. Specifically, we discovered that the Nova family of RNA-binding proteins are activity-dependent and are essential for the maturation of somatostatin interneurons, as well as their afferent and efferent connectivity. Moreover, in somatostatin interneurons, Nova2 preferentially mediates the alternative splicing of genes required for axonal formation and synaptic function. Hence, our work demonstrates that the Nova family of proteins are centrally involved in coupling developmental neuronal activity to cortical circuit formation.

Keywords: Interneuron; Neurodevelopment; Activity; Alternative splicing; Connectivity; Synapse; Nova1; Nova2.

INTRODUCTION

Somatostatin cortical interneurons (SST cINs) constitute ~30% of all inhibitory interneurons in the cerebral cortex. They are crucial for gating the flow of the sensory, motor, and executive information necessary for the proper function of the mature cortex (Fishell and Rudy, 2011; Kepecs and Fishell, 2014; Tremblay et al., 2016). In particular, Martinotti SST cINs, the most prevalent SST cIN subtype, are present in both the infragranular and supragranular layers of the cortex and extend their axons into Layer 1 (L1) (Lim et al., 2018; Muñoz et al., 2017; Nigro et al., 2018). They specifically target the distal dendrites of neighboring excitatory neurons, thus providing the feedback inhibition necessary for modulating dendritic integration (Adler et al., 2019; Favuzzi et al., 2019; Kapfer et al., 2007; Silberberg and Markram, 2007). These roles are dependent upon the remarkable ability of SST cINs to form specific synaptic connections with select excitatory and inhibitory cell types during development.

The mechanisms responsible for generating the precise functional connectivity of SST cINs are poorly understood. Early neuronal activity has emerged as an important cue in directing the maturation of cINs (Wamsley and Fishell, 2017). In addition, recent work has implicated activity as being centrally involved in alternative splicing (Eom et al., 2013; Furlanis and Scheiffele, 2018; Iijima et al., 2011a; Lee et al., 2007; 2009; Mauger et al., 2016; Quesnel-Vallières et al., 2016; Vuong et al., 2016; 2018; Xie and Black, 2001). However, whether these processes are coupled within interneurons has not been explored.

The Nova family of RNA-binding proteins (Nova1 and Nova2) have been shown to control the splicing and stability of transcripts encoding a variety of neurotransmitter receptors, ion channels, and transmembrane cell adhesion molecules known to affect synaptogenesis and excitability (Dredge and Darnell, 2003; Eom et al., 2013; Saito et al., 2016; 2019; Ule et al., 2005; 2003a; 2006; Yano et al., 2010). Notably both Nova1 and Nova2 are strongly expressed within cINs during the period of synaptogenesis and as such represent promising effectors that may direct the maturation of SST cINs.

Here we report that neuronal activity is vital for the proper establishment of both afferent and efferent SST cIN connectivity. We show that the conditional loss of *Nova1* or *Nova2* largely

phenocopies the effect of dampening activity during circuit assembly, leading to a loss of excitatory synaptic afferents onto SST cINs, as well as their efferent inhibitory output. At a molecular level these changes are mediated by a Nova-dependent program, which controls the alternative splicing of mRNAs encoding for pre- and post-synapse proteins. Demonstrating a direct link between activity, Nova function and synaptogenesis, overexpression of *Nova2* within SST cINs dramatically increases synaptogenesis, a phenotype that can be suppressed by damping neuronal activity within these cells. Thus, our work indicates that early activity is required for the proper establishment of SST cIN connectivity and maturation through a Nova-dependent mechanism.

RESULTS

Neuronal activity affects the synaptic development of SST cINs

The cortex exhibits a variety of dynamic network activity patterns during cortical synaptogenesis (Allene and Cossart, 2010; Garaschuk et al., 2000; J. W. Yang et al., 2009). These are comprised by both spontaneous and sensory evoked events (Garaschuk et al., 2000; Minlebaev et al., 2011; J.-W. Yang et al., 2012). While cINs are recruited by these activities (Cossart, 2011; Le Magueresse and Monyer, 2013), whether this influences SST cIN development has not been fully established. To address the impact of activity on these cINs, we chose to selectively and cell-autonomously dampen or augment their excitability during the first few weeks of development. This represents a perinatal period in cIN development during nascent circuit formation, where they are robustly forming or losing synaptic contacts (Allene et al., 2008; Minlebaev et al., 2011; J.-W. Yang et al., 2012; J. W. Yang et al., 2009). SST cINs in the primary somatosensory cortex (S1) were targeted using AAV viral injections in mice carrying an *SST^{Cre}* allele and a conditional compound synaptophysin1-eGFP (Syp-eGFP) construct, which functions as a presynaptic reporter (i.e *SST^{cre};R26R $^{LSL\text{-}tTa}$;Tg-TRE::Syp-eGFP*, Figure1A) (Basaldella et al., 2015; Li et al., 2010; Wamsley et al., 2018). To modulate the activity of SST cINs, these mice were injected at P0 with Cre-dependent AAVs that drive the expression of either KIR2.1 or NaChBac channels along with an mCherry reporter (Figure 1A, B). Both channels are voltage-sensitive and have proven to be useful tools to manipulate cellular excitability. The KIR2.1 channel is an inward rectifying potassium channel, which upon overexpression lowers the resting membrane potential towards the reversal potential of K^+ (~90mV) (Bortone and Polleux, 2009; De Marco García et al., 2011; Karayannis et al., 2012; Priya et al., 2018; Yu et al., 2004), thus reducing neuronal excitability. The NaChBac channel has an activation threshold that is 15mV more negative than endogenous voltage-gated Na^+ channels and remains open for 10 times longer (Lin et al., 2010) and therefore augments excitability. To assess the development of the synaptic efferents of infected SST cINs, we allowed pups to mature until juvenile age (P21). Mice were then sacrificed and underwent immunohistochemistry (IHC) to visualize mCherry, Syp-eGFP and gephyrin, followed by confocal

imaging and axonal and puncta analysis (Ippolito and Eroglu, 2010). We quantified the density of axon arbors of SST cINs by assessing the number of the mCherry-labeled axons restricted to L1 (Figure 1C). We found that the expression of KIR2.1 in SST cINs significantly reduced axonal density and arborization (141.71±90.45 control (ctl) axon/um^2 vs 39.65±13.63 KIR2.1 axon/um^2 , pVal= <0.00001) whereas the expression of NaChBac increased the axonal density in L1 compared to controls (141.71±90.45 ctl axon/um^2 vs 203.5±80.84 NaChBac axon/um^2, pVal= 0.01) (Figure 1B, C). Next, we quantified SST synapse density identified through the colocalization of the virally mediated mCherry reporter, Syp-eGFP and the postsynaptic marker gephyrin (mCherry+/GFP+/gephyrin+ puncta), as a proxy for synaptic contacts (Figure 1D, Ippolito and Eroglu, 2010). In SST cINs, KIR2.1 expression resulted in a significant reduction of L1 SST cIN efferent synaptic puncta in comparison to control cells (0.109±0.009 puncta/um^2 ctl vs 0.049±0.006 puncta/um^2 KIR2.1, pVal= 0.0001) (Figure 1E). By contrast, the overexpression of NaChBac within SST cINs resulted in a robust increase in L1 synaptic puncta (0.109±0.009 puncta/um^2 ctl vs 0.218±0.030 puncta/um^2 NaChBac, pVal= 0.008) (Figure 1D, E). These results suggest that activity has a profound effect on the density of SST cIN axons and synapses. Dampening excitability decreases the number of efferent synaptic structures and axonal arbors of SST cINs, while augmenting it increases both.

Neuronal activity influences alternative splicing and Nova expression within SST cINs

A growing number of studies indicate that activity-dependent alterative splicing (AS) contributes to the regulation of gene expression and the fine-tuning of transcriptional programs related to synaptic refinement (Eom et al., 2013; Iijima et al., 2011b; Mauger et al., 2016; Quesnel-Vallières et al., 2016; Vuong et al., 2016). This prompted us to test whether neuronal activity itself changes the level of AS within SST cINs during circuit formation. To do so, we used electro-convulsive shock (ECS) during peak synaptogenesis (P8) in *SST^{Cre};Ai9* mice. The ECS method generates an acute and reproducible increase in neuronal activity *in vivo* (Guo et al., 2011; Ma et al., 2009), resulting in increased expression of immediate early genes (IEG) such as, *Fos*, *Egr1*, *Npas4* and *Arc* (Figure S1A-E), analogous to that

observed with KCl treatment *in vitro* but with the added advantages of being *in vivo* and transient. Two to three hours following ECS, we isolated SST cINs from the S1 cortex of *SST^{Cre};Ai9* animals using fluorescence activated cell sorting (FACS) (Figure 2A). Sorted SST cINs were used to prepare cDNA libraries that were subsequently sequenced in order to investigate changes in AS (spliced exon: SE, mutually exclusive exons: MXE, retained intron: RI, alternative 5' splice site: A5, alternative 3' splice site: A3) (Figure2A, right). We found 312 transcripts differentially spliced between sham and ECS (FDR<0.05, $|\Delta\psi|\geq 0.1$ threshold), comprised by 139 SE events (82 included and 57 excluded exons), 66 RI events (53 included and 13 excluded introns), 31 MXE events (26 included and 29 excluded exons), 13 A5 events (12 included and 1 excluded exons), and 39 A3 (16 included and 23 excluded exons) (Figure 2B).

Utilizing the SST cIN transcriptome as a reference, we performed gene ontology (GO) analysis to ask if the genes subject to differential AS were enriched for specific functional categories within these neurons. GO analysis of the genes that underwent activity-dependent AS belong to specific ontological categories, such as synapse maturation, synaptic transmission, and axonal growth (Figure 2E). For example, we observed and validated (Table S3) that within activity stimulated SST cINs the *Nrxn1* mRNAs exclude exon 10. Notably, this exon lies within a laminin-protein coding domain important for the cell adhesion properties of Nrxn1 at the synapse (Figure 2C, sham, grey vs ECS, green). We next asked whether the activity-dependent AS genes formed a protein-protein interacting network (PPI) based on previously established direct protein interactions *in vivo* (Rossin et al., 2011). Notably, the genes subjected to activity-dependent AS within SST cINs form highly connected networks illustrating they likely function together to support pre-synaptic vesicle function (Figure 2F, pink), post-synaptic organization and receptor-associated synaptic components (Figure 2F, blue) (pVal<0.0009, 1000 permutations). These genes among others include: *Hspa8, Nrxn1, Syngap1, Cacna1c, Ppp3ca,* and *Grin1* (Figure 2F). These results indicate that augmenting activity within SST cINs during nascent circuit development robustly increases AS events and a majority of the spliced mRNAs are genes specifically related to axonal development and synaptic transmission (Figure2F, pink and blue, respectively).

We next sought to identify RNA binding proteins (RNABPs) that could mediate activity-dependent AS events within SST cINs. To do so, we utilized the RNAseq experiments described above (sham vs. ECS) to perform a motif enrichment analysis that utilizes position probability matrices of binding motifs from 102 RNABPs (i.e. PTBP1/2, FUS, ELAVL4, SRRM4, Rbfox1, FMR1, Nova1, Nova2) (Liu et al., 2017; Park et al., 2016; Y. Yang et al., 2016). Previous HITS-CLIP analysis has revealed that Nova1 and Nova2 share an almost identical RNA-binding domain (YCAY) (Licatalosi et al., 2008; Ule et al., 2006; 2003b; Yuan et al., 2018a). Strikingly, the Nova-binding motif was found to be significantly enriched within activity-dependent targets and at a higher frequency than other neuronal splice factors (i.e. Sam68 (KHDRBS1), SLM2 (KHDRBS2), and Rbfox1) (pVal<0.0001) (Figure 2D). This finding implicates Nova proteins as playing a fundamental role in directing SST cIN activity-dependent AS.

Neuronal activity during cortical development influences the expression and localization of Nova proteins in SST cINs

We next examined the expression of Nova1 and Nova2 within SST cINs across development and whether their expression is affected by changes in neuronal activity. Utilizing IHC and genetic fate mapping, we observed that the expression of the Nova family (Nova1 and Nova2) of splice regulators begins within cIN populations soon after they become postmitotic and expressed in 100% of SST and PV cINs by adulthood (Figure S2A, B). For comparison we also examined Nova expression in excitatory cells (Fig 3B) and 5HT3aR cINs (Figure S2B, C) within this same region. To specifically examine the expression of Nova1 and Nova2 during SST cIN synaptogenesis, we performed quantitative-PCR (qPCR) on FACS isolated cINs from the S1 cortex of *Tg-Lhx6::eGFP* mice at P2, P8, and P15. The *Tg-Lhx6::eGFP* mice express eGFP in both SST and Parvalbumin (PV) cINs soon after they become postmitotic. We found that both *Nova1* and *Nova2* are expressed within all SST and PV cINs across the first two weeks of postnatal development, coinciding with nascent circuit development (Figure 3A, Figure S2B). Interestingly, at P2 the expression of both Nova1 and Nova2 in cINs is significantly higher

than in cortical excitatory neurons (cExt, Figure 3B). Taken together, we find that both Nova1 and Nova2 splice factors are highly expressed highly in all SST cINs during circuit integration and may therefore control integral aspects of their development through activity-dependent alternative splicing.

We next investigated whether Nova1 and Nova2 are activity-regulated within SST cINs by examining both their expression and localization during the peak of nascent circuit integration. To do so, we subjected *SST^{Cre};Ai9* mice to ECS during synaptogenesis (Figure 3C). Next, we performed qPCR for *Nova1* and *Nova2* within FAC sorted cINs from S1 cortex of either sham or ECS-treated animals. Following 1.5 hours post seizure-induction (1.5 HRPS), we found that the mRNA expression levels of both *Nova1* and *Nova2* were increased in ECS-treated SST cINs compared to controls (*Nova1:* 28.4±5.59 ECS vs 7.61±0.25 sham; *Nova2* pVal=0.002*:* 10.32±1.80 ECS vs 6.59±0.28 sham pVal=0.005, Figure 3D). Next, we probed Nova1 and Nova2 protein levels using western blot of sorted SST cINs from S1 cortex. Consistent with an activity-mediated upregulation in *Nova* expression, we found a significant increase in both Nova1 and Nova2 protein levels (0.824±0.0412 pixel density Nova1 sham vs 5.62±0.969 pixel density Nova1 2HRPS, pVal= 0.038 and 0.997±0.409 pixel density Nova2 sham vs 5.7±0.582 pixel density Nova2 2HRPS, pVal= 0.022, pixel densities normalized to ß-Actin) (Figure 3E-F). Thus, these results confirm an increase in Nova mRNA and protein expression in SST cINs following an acute increase in neuronal activity.

Following seizure activity Nova proteins have been shown to translocate into the nucleus within excitatory neurons (Eom et al., 2013). We next sought to explore whether manipulating activity also influences Nova intracellular localization in SST cINs (Figure 3G-K). We hypothesized that an activity-mediated increase would direct Nova proteins to the nucleus. We therefore analyzed the ratio of SST cINs with Nova expression within the nucleus versus the cytoplasm following ECS (Figure 3G-I) or after constitutive activity-modulation across the first postnatal month (DIO:AAV injections of KIR2.1 or NaChBac into *SST^{cre}* animals at P0) (Figure 3G,J-L). First, we examined Nova localization using IHC 2HRPS following ECS within the S1 cortex of P8 *SST^{Cre};Ai9* mice (Figure 3G-H). We quantified the proportions of SST cINs that express Nova proteins most prominently within the nucleus versus the

cytoplasm by taking multi-Z-stack images of SST cINs and utilizing DAPI to demark the nuclear boundary. We found that Nova localization was observed in three basic patterns in SST cINs: restricted to the nucleus, cytoplasm restricted, or a combination of both nuclear and cytoplasmic expression (Figure 3G). At P8, in the majority of SST cINs, Nova is either restricted to the cytoplasm or expressed in both the nucleus and cytoplasm (Figure 3I). Following an acute increase in activity (ECS), we found a significant increase in the ratio of nuclear to cytoplasmic Nova protein within SST cINs (0.948±0.055 ratio in sham versus 3.65±0.465 ratio in ECS, pVal= 0.001, Figure 3H, I). Next, by utilizing the same analytical approach, we examined Nova protein localization in S1 of P21 mice that express either KIR2.1 or NaChBac along with an mCherry reporter (Figure 3J, K). We found a substantial increase in the ratio of SST cINs that localized Nova protein in the nucleus compared to the cytoplasm in NaChBac-expressing compared to control cells (4.75±0.678 ratio control vs 40.91±8.41 ratio NaChBac, pVal= 0.0004) (Figure 3K, left). In contrast, we found a robust decrease in the ratio of nuclear to cytoplasmic Nova protein within SST cINs injected with KIR2.1 (4.75±0.678 ratio control vs 0.265±0.104 ratio KIR2.1, pVal= <0.0001) (Figure 3K, right). Most striking, we also observed more than half of SST cINs subjected to KIR2.1 expression have substantially reduced levels of Nova protein expression (Figure 3L-N, pVal= 0.0303). Altogether these data indicate that during synaptogenesis Nova protein expression and localization within SST cINs is strongly modulated by acute or persistent changes in activity.

Nova1 and Nova2 control distinct AS networks within SST cINs

To address whether Nova1 and Nova2 differentially affect connectivity and maturation**,** we asked what AS networks they control within SST cINs during development. Given that they share a very similar RNA-binding motif and are found associated with one another in vivo, they were thought to function cooperatively (Licatalosi et al., 2008; Racca et al., 2010; Yuan et al., 2018b). However recently, it has been shown that in addition to their synergistic roles, Nova1 and Nova2 proteins each control distinct

AS gene networks (Saito et al., 2019; 2016). We thus chose to examine changes in AS within SST cINs in Nova1, Nova2 or compound conditional knockout mice (Saito et al., 2019; Yuan et al., 2018b). Using FAC sorting, we isolated SST cINs from *SST^{Cre};Nova1$^{F/F}$* or *SST^{Cre}*; *;Nova2$^{F/F}$* or *SST^{Cre};Nova1$^{F/F}$*; *Nova2$^{F/F}$* mice on an Ai9 reporter background (referred to henceforth at *SST-Nova1*, *SST-Nova2* and *SST-dKO,* respectively*)* at P8 (Figure S3A). We prepared cDNA libraries from FAC sorted SST cINs, performed RNA sequencing and assessed AS changes between control SST cINs versus each of these mutant alleles. Compared to wild type controls, *Nova1* loss resulted in 124 altered AS events (43 included and 81 excluded), *Nova2* loss lead to 339 altered AS events (122 included and 217 excluded) and double mutants exhibited 270 altered AS events (108 included and 162 excluded) (FDR < 0.05) (Figure S3B). These results illustrate that within SST cINs, the loss of *Nova2* results in the largest number of changes in mRNA splicing events compared to compound loss of either *Nova1* or both *Nova* genes. We next assessed the overlap of changes in AS events observed within each mutant (Figure S3C-E). We found the number of alterations in *SST-Nova2* AS events that overlap with *SST-dKO* is almost three times higher than that observed when comparing the overlap between *SST-dKO* and *SST-Nova1* (i.e. 62 altered *SST-Nova2* AS events coincided with the 162 observed in *SST-dKO* versus an overlap of only 25 AS events that were altered in *SST-Nova1* mutants, Figure S3DE). By contrast, less than 15% of the altered *SST-Nova1* AS genes overlap with changes observed in *SST-Nova2* mutants (i.e. only 28 of the 217 *SST-Nova2* events were altered in *SST-Nova1* mutants) (Figure S3C, D). Interestingly, *SST-dKO* mutants exhibited less altered splicing events than the single *SST-Nova2* mutant, suggesting that some inclusion and exclusion AS events are antagonistically directed by Nova1 and Nova2.

To infer their specific biological functions, we performed GO analysis on the altered AS events from each mutant and then asked whether the affected AS events form direct PPI networks. GO analysis of the *SST-Nova1* targets did not result in any significant enrichment of specific functional categories (below an FDR of 0.05) however it did organize genes into categories such as RNA binding, ion binding, and catalytic activity (Figure S3F). *SST-Nova1* AS genes formed a relatively indistinct small

sparse PPI network (pVal<0.09) representing vesicle-transport and nucleic-acid binding pathways (Figure S3I, pink shaded). In contrast, *SST-Nova2* and *SST-dKO* AS genes organized into several shared significant GO categories such as neuron projection, axon, cell-cell junction, and synaptic function (FDR <0.05) (Figure S3G, H). *SST-dKO* AS genes also organized into some unique categories, which were involved in postsynaptic specialization, dendrite, and synaptic vesicle membrane (FDR <0.05) (Figure S3H). We next asked if the AS genes affected in *SST-Nova2* and *SST-dKO* were predicted to function together in a PPI network representing specific biological processes (Figure S3I-K). Perhaps not surprisingly both formed highly connected significant PPI networks (pVal < 0.0009, 1000 permutations) representing multiple pathways for vesicle-transport, pre- and post-synaptic function and organization, as well as Ca^{2+} signaling (Figure S3J, K, pink and green respectively). Interestingly, the PPI network for *SST-Nova2* uniquely includes numerous glutamate receptors and their adaptors, respectively (i.e. Grin2b, Grik1, Gria3, Grm5 and Grip1, Sharpin, Dlg2) (Figure S3J, highlighted pre-synaptic genes in pink and post-synaptic genes in green). Altogether these results suggest that considering the *Nova* family as a whole, *Nova2* (compared to *Nova1*) is the main driver of AS and importantly, may be most relevant for synaptic development of SST cINs.

***SST-Nova1 and SST-Nova2* mutants have impaired afferent and efferent connectivity.**

To confirm our predictions from the AS analysis of conditional *Nova* mutants, we next sought to determine the effect of the loss of *Nova1* and *Nova2* on SST cIN synaptic development and function. To this end, we assessed the requirement for *Nova1* and/or *Nova2* for both the anatomical connectivity and physiological properties of SST cINs. *SST-dKO* mice were small in size and while generated at Mendelian ratios, many died as early as P8 and often exhibited seizures (Figure S4A and results not shown). In the single cKO mutants, we used IHC to quantify the density of SST cIN efferent synapses, defined as the apposition of VGAT+ (vesicle GABA transporter) and gephyrin+ puncta from a SST cIN axon within L1 of the S1 cortex at P8 (Figure 4A, black asterisks mark example puncta). We found that both *SST-Nova1* (0.281±0.041 puncta/um^2 *SST-Nova1* vs 0.454±0.037 puncta/um^2 ctl, pVal=0.003)

and *SST-Nova2* (0.197±0.016 puncta/um^2 *SST-Nova2* vs 0.454±0.037 puncta/um^2 ctl, pVal=<0.0001) exhibited a significant reduction in SST+ synapses compared to control SST synapses within L1 (Figure 4B). To confirm the synaptic phenotype observed, we recorded the inhibitory outputs from SST cINs onto pyramidal cells in L2/3 and L5 using a conditional channelrhodopsin mouse line (*Ai32$^{F/F}$*) crossed with *SST-Nova1*, *SST-Nova2* or SST-control mice (Figure 4C). We observed a significant reduction in the light evoked IPSC peak amplitude in both *SST-Nova1* (283±36pA in *SST-Nova1* vs 623±120pA in ctl, pVal=0.0037), as well as *SST-Nova2* (340±85pA in *SST-Nova2 vs* 766±211pA ctl, pVal=0.0021), confirming that the anatomically observed reduction in synaptic output density is functionally significant in both mutants (Figure 4D *SST-Nova1* top orange trace, *SST-Nova2* pink trace bottom). While both *SST-Nova1* and *SST-Nova2* leads to a reduction in both the density of synaptic efferents and their inhibitory function, loss of *Nova2* has a bigger impact on efferent connectivity within SST cINs than *Nova1* (one-way ANOVA, pVal=0.0001).

We also investigated whether the density of excitatory synapses onto SST cINs is affected by the loss of *Nova1* or *Nova2*. We performed IHC for Vglut1 (vesicular glutamate transporter) and Homer1c on *SST-Nova1* and *SST-Nova2* dendrites within the S1 cortex at P8 (Figure 4E, black asterisks mark example puncta). We quantified the density of putative excitatory synapses by the overlap of Vglut1+ and Homer1c+ puncta onto mCherry+ dendrites of SST cINs. We found that the number of putative excitatory afferent synapses onto *SST-Nova1* and *SST-Nova2* is significantly reduced compared to control SST cINs (0.144±0.016 puncta/um^2 *SST-Nova1* vs 0.207±0.022 puncta/um^2 ctl, pVal= 0.028 and 0.137±0.013 puncta/um^2 *SST-Nova2* vs 0.207±0.022 puncta/um^2 ctl, pVal= 0.012) (Figure 4F). To examine whether these anatomical abnormalities observed in *SST-Nova1* and *SST-Nova2* mutants affected synaptic function, we performed whole-cell patch clamp recordings to measure miniature excitatory postsynaptic currents (mEPSCs) within SST cINs (Figure 4G). In accordance with the puncta analysis, both *SST-Nova1* and *SST-Nova2* exhibited significant reductions in the mEPSC frequency (*SST-Nova1*: 1.16± 0.08 Hz vs *SST-Nova2*: 0.39±0.05 Hz vs ctl: 2.43±0.2 Hz, pVal=0.0025, Figure 4H). In addition, we observed a significantly increased mEPSC amplitude in *SST-*

Nova2 (*SST-Nova2*: -40±15.7pA vs *SST-Nova1*: -30.12±13.15pA vs ctl: -30.36±13.34pA, pVal=0.0.0001, Figure S4D-G). Thus, while *SST-Nova2* cINs have a striking reduction in their excitatory inputs, the remaining excitatory synapses are functionally stronger than *Nova1* or control cINs. Moreover, the intrinsic properties of both *cKO* alleles were differentially affected. Specifically, we observed that the rheobase was significantly lower for *SST-Nova2* compared with either controls or *SST-Nova1* (*SST-Nova2*: 25±3pA vs ctl:120±25pA vs *SST-Nova1:* 70±15pA;. pVal=0.01, Table S2). As rheobase is a measurement of the minimum current required to produce an action potential, *SST-Nova2* cIN*s* are potentially compensating for the loss of excitatory synapses by lowering the minimal current amplitude required for depolarization. Other intrinsic physiological properties are summarized in Table S2. Altogether these results solidify the role of both Nova1 and Nova2 in the synaptic development of SST cINs. Furthermore, consistent with the AS analysis, these results suggest that within SST cINs *Nova2* has a larger impact on the changes in synaptic connectivity compared to *Nova1*.

Nova RNA binding proteins control activity dependent AS in SST cINS during development

Given that activity increases the expression level and nuclear localization of both Nova proteins, we hypothesized that their loss would result in changes in activity-dependent AS. To this end, we repeated our investigation of how Nova-dependent AS isoforms are altered in mutant mice. This time we examined the changes specifically following ECS within SST cINs during synaptogenesis *in vivo*. 2-3 hrs following ECS, we isolated SST cINs from *SST-dKO* mice (Figure 5A). Following augmentation of neuronal activity, we found that the loss of both *Nova* genes results in the differential splicing of 346 transcripts (FDR<0.05, $|\Delta\psi|\geq 0.1$). These are broken down into 166 SE events (106 included and 60 excluded exons), 72 RI events (51 included and 21 excluded introns), 70 MXE events (37 included and 33 excluded exons), 9 A5 events (7 included and 2 excluded exons), and 30 A3 (9 included and 21 excluded exons) (Figure 5B). Independent fluorescent RT-PCR amplifications with primers flanking the alternatively spliced segments confirmed the observed AS changes. We were able to validate 70% of targets tested (Table S3). For example, we validated the activity-dependent inclusion of exon 14 in

Syngap1, a gene associated in multiple disorders including epilepsy and important for excitatory post-synaptic function (Figure 5C, D). As predicted from RNAseq, SST cINs subjected to acute increases in activity from *SST-dKO* animals, compared to control SST cINs, exhibit a significant reduction in the expression of *Syngap1* exon 14 (Figure 5D).

We found the majority of genes which undergo activity-induced Nova-dependent differential splicing were significantly enriched for GO categories such as pre-synaptic vesicular function, synapse organization, synaptic transmission, and neuronal growth (Figure 5E). Many of the genes within these categories are known to have important functions for axon organization and synaptogenesis such as, *Nrxn1, Nrxn3, PlxnA2,* and *EphA5*. Interestingly, the activity-dependent Nova AS targets were strikingly enriched for excitatory post-synaptic specializations such as, *Shank1*, *Syngap1, Dlg3, Grin1* and *Gria1*. Furthermore, these genes are predicted to function together in a direct PPI network representing specific pre-synaptic and post-synaptic biological processes (direct network pVal= 0.0009, 10000 permutations, Figure 5F). For example, the loss of *Nova* leads to an altered activity-dependent splicing program of multiple genes important to NMDA receptor-mediated signaling (Grin1) connected with PSD organization (i.e. Dlg3, Shank1) and Ca^{2+} -dependent signaling (i.e Hras, Rapgef1) (Figure 5F).

In sum, the activity-mediated Nova-dependent AS changes within SST cINs are central for fine-tuning of synaptic and axonal development. We previously found that another important RNABP, Rbfox1, influences axonal development and also shuttles from the cytoplasm to the nucleus upon increase in activity in SST cINs (Lee et al., 2009; Wamsley et al., 2018). However, upon comparing the activity-dependent splicing programs within SST cINs of Rbfox1 (69 activity-dependent events) to Nova1/2 (346 activity-dependent events), we found Nova proteins control a much larger number of activity-dependent splicing events. This supports our hypothesis that Nova proteins are key players in the control of activity-dependent AS (Figure S5A).

Nova2 overexpression within SST cINs augments axonal growth and synaptic formation in an activity dependent manner

Activity increases both the expression of Nova proteins as well as synapse formation; while conversely there is a striking decrease in synaptogenesis after loss of Nova function. Moreover, from our analysis of SST cIN cKOs, it was evident that of the two Nova proteins, *Nova2* has the more profound effect on the AS of genes involved in synaptogenesis. We therefore examined whether over expression (OE) of *Nova2* alone could phenocopy the observed changes in connectivity within SST cINs. To that end, we overexpressed *Nova2* specifically in SST+ neurons using an AAV virus (AAV-TRE-Nova2-mCherry) together with a Cre-dependent synaptophysin1-eGFP virus (AAV-hSyn-DIO-Synaptophysin1-eGFP) in SST^{Cre}:$tTA^{F/F}$ mice within the S1 cortex (Figure 6A). Remarkably, the overexpression of *Nova2* had a similar effect as increasing activity; the axonal density in L1 of SST cINs was significantly increased compared to controls (118.5±53 axon/um^2 controls vs 198.2±23 axon/um^2-*Nova2* OE; pVal=0.0012) (Figure 6B, C, E). Additionally, this increased axonal density was associated with increased synaptogenesis. We quantified the density of putative synaptic puncta as defined by the juxtaposition of presynaptic Syp-eGFP from the OE *Nova2* SST neurons colocalized with gephyrin (0.026±0.0031 synaptic puncta/um^2 in ctl vs 0.055±0.01 synaptic puncta/um^2 in the case of Nova2 OE; pVal=0.04) (Figure 6F, G, I). Moreover, as in the case of increasing activity (either constitutively, NaChBac, or acutely, ECS), the nuclear localization of Nova was robustly increased when *Nova2* was overexpressed in the SST cINs (Figure 6J, L).

We next asked whether suppressing activity would affect the increased axogenesis and synaptogenesis observed with the *Nova2* OE. We expressed KIR2.1 in SST cINs as described earlier, together with the *TRE-Nova2-mCherry* in the S1 cortex (Figure 6A). The dual expression of Nova2 OE and KIR2.1 within SST cINs prevented the increased axogenesis that was observed with *Nova2* OE alone (198±23 axon/um^2 in *Nova2* OE vs 30.37±10.51 axon/um^2 in the case of Nova2 OE&KIR2.1, pVal=0.0053) (Figure 6D, E). As observed with KIR2.1 alone, this decreased axogenesis also corresponded with decreased synaptogenesis (0.055±0.011 synaptic puncta/um^2 in *Nova2* OE vs 0.024±0.007 synaptic puncta/um^2 Nova2OE+KIR2.1, pVal=0.0042) (Figure 6H, I). Additionally, the increased nuclear localization of Nova that was observed with the *Nova2* OE was abolished when the

activity of the cells was cell-autonomously reduced using KIR2.1 (Figure 6K, L). Perhaps most strikingly, as with our initial KIR2.1 experiment, the levels of Nova2 protein despite being constitutively OE were strongly reduced in cells co-expressing KIR2.1 (Figure 6K). This provides strong evidence that the stability of Nova protein is dependent on the level of basal activity within SST cINs.

Discussion

In the present study, we have examined the effect that both neuronal activity and the Nova RNABPs have on the synaptogenesis of SST cINs. Our analysis began with the observation that activity levels strongly influence the maturation of SST cINs. Acutely evoking activity during circuit integration with ECS resulted in both transcriptional and translational upregulation of Nova proteins. This was accompanied by a striking change in AS of synaptic genes and synaptogenesis within SST cINs. We then systematically examined whether a causal relationship exists between these three observations.

Our results indicate that within this interneuron population, particularly during periods of circuit maturation, excitation levels correlate with changes in AS and the formation of afferent/efferent connectivity. These events appear to be tightly linked to Nova function, as the expression, localization and splicing activity of both Nova1 and Nova2 proteins are strongly modulated by activity. Examination of how splicing events are impacted by *Nova* single and compound cKOs in SST cINs demonstrate that developmental RNA splicing events in these cells are particularly impacted by the loss of *Nova2.* This is mirrored by the magnitude in reduction of excitatory input and inhibitory output within SST cINs, accompanied by a structural decrease in their synaptic contacts. Conversely, over-expression of *Nova2* in SST cINs greatly enhances synaptogenesis, a phenomenon that can be suppressed by simultaneous dampening of excitability. Together these findings demonstrate that activity is coupled to synaptogenesis by a mechanism involving Nova-mediated splicing of synaptic proteins.

We and others have shown that activity regulates programmed cell death {Priya:2018hc, Marin:2016bi, Denaxa:2018iu, Wong:2018fu}. However, we observed no indication that the loss of *Nova2* impacted SST cIN survival. In addition, we observed that NaChBac and KIR2.1 could modulate

synaptogenesis in SST cINs both during and after the peak of cell death in this region (data not shown). Conversely, the number of phenotypic changes observed in conditional *Nova* loss of function mutants suggests that these genes have effects beyond synaptogenesis. Nova2, in particular, also targets genes involved in protein trafficking to the membrane, cell-cell signaling, and neurotransmitter/ion channel function, indicating it influences multiple aspects of SST cIN maturation. In addition, prior work from the Darnell lab has demonstrated a role for Nova2 in both migration and axonal pathfinding within the cortex, spinal cord and brain stem (Saito et al., 2016; Yano et al., 2010). Taken together clearly much remains to be understood concerning the role Nova proteins play during development in specific brain regions, circuits, and cell types.

While Nova function is a core regulator of alternative splicing in SST cINs, it represents only one of a host of RNABPs utilized both within this cell type, as well as across neurons in general. A recent study demonstrated that within the mature CNS many classes of neurons, including SST cINs, can be classified both by their expression levels of RNABPs and their corresponding repertoire of alternatively spliced mRNAs (Furlanis et al., 2019). Comparison of their work to our present findings illustrate that both the expression of RNABPs and the patterns of AS are strongly regulated across development and are responsive to changes in neuronal activity. RNA binding splice factors have previously been shown to promote alternative splicing of synaptic proteins in response to neuronal depolarization and Ca^{2+} signaling (Eom et al., 2013; Mauger et al., 2016; Quesnel-Vallières et al., 2016; Vuong et al., 2016), For example, previous research demonstrated that the splicing of neurexins, a gene family known to function in synaptogenesis, are mediated through the actions of the SAM68 splicing factor (Iijima et al., 2011b). Similarly, It has also been illustrated that neuronal activity reduces the expression of the SRRM4 RNA-binding protein, which resulted in altered RNA splicing and a corresponding decrease in excitatory synapses (Quesnel-Vallières et al., 2016). As such AS represents a largely unexplored but central genetic mechanism, capable of directing cell-type specific development and specification.

Understanding both the repertoire of splice factors and the cell-specific patterns of splicing across development will undoubtedly provide further insight into how AS influences cIN development.

One could imagine systematically examining the role of these differential splice mRNA variants through combinatorial knockdown or over-expression. However, this would be technically challenging, even if restricted to only those that are Nova-dependent. As we show here many of these AS genes have been shown to function together (PPI networks), knocking down one or a few would most likely result in the same phenotype. In addition, the abundance of the specific splice forms of different genes within SST cINs is relative rather than absolute. Such that the identity, amount, and function of the genes that make up a cell's alternatively spliced gene network will change dependent on cell identity and state (i.e. developmental period, neuronal activity, etc). Further complicating matters, activity also affects the overall transcription level of these same genes. As a result, the abundance of particular splice forms co-vary as a function of both transcription and AS. Taken together, this argues that conditional removal of RNABPs, such as Nova2, is a more biologically relevant approach to understanding the role of AS within discrete cell types.

Our results show a clear interdependence between activity, Nova function and synaptogenesis in SST cINs. The dual observations that 1) *Nova2* over-expression is sufficient to increase synaptogenesis and 2) that co-expression of KIR2.1 can suppress this effect, demonstrate that the two are functionally coupled. Most obviously this appears to be regulated through an activity-dependent increase in *Nova* expression (see model Figure 6M). When SST cIN activity is increased with ECS or with NaChBAC expression, *Nova* transcripts as well as protein are upregulated and shuttled to the nucleus. The mechanisms for activity-dependent changes in Nova expression and localization are unknown. It is possible that the *Nova* gene loci may contain binding sites for immediate-early-genes (i.e. cFOS, Jak/Jun, EGF) or specific activity-dependent transcription factors (i.e. NPAS4, Satb1). With regard to control of its localization, previous work has discovered a nuclear-localization signal (NLS) within the Nova protein domains. It is however unknown whether their activation is mobilized by splicing or post-translational modifications. For instance, *Rbfox1* undergoes activity-dependent mRNA splicing that results in exposure of an NLS and localization to the nucleus (Lee et al., 2009; Wamsley et al., 2018). Furthermore, our results indicate that activity itself regulates Nova2 RNA and protein stability.

In the presence of KIR2.1, the levels of Nova protein appear to be dramatically reduced, even when *Nova2* is over-expressed. In this latter context, clearly *Nova2* levels are not constrained by mRNA production. These results indicate that the stability of Nova protein is at least partly dependent on activity. Taken together, these findings indicate that there exist multiple mechanisms by which cell activity is coupled to Nova function and AS within SST cINs. Given its broad expression and the strong phenotypes associated with both conditional and global *Nova* loss of function, studies of this RNABP will no doubt provide further insights into their contribution to normal and disease brain function.

CONTACT FOR REAGENT AND RESOURCE SHARING

Please contact GF for reagents and resources generated in this study.

EXPERIMENTAL MODEL AND SUBJECT DETAILS

- **Mouse maintenance and mouse strains**

All experimental procedures were conducted in accordance with the National Institutes of Health guidelines and were approved by the Institutional Animal Care and Use Committee of the NYU School of Medicine and Harvard Medical School. Generation and genotyping of, *SST*^{Cre} (Taniguchi et al., 2011), *RCE*^{eGFP}(Sousa et al., 2009), *Lhx6* BAC transgenic (referred to as tg*Lhx6;eGFP*) (Gong et al., 2003), *Nova1*$^{LoxP/LoxP}$ (Yuan et al., 2018a) , *Nova2*$^{LoxP/Lox}$(Saito et al., 2019), TRE-Bi-SypGFP-TdTomato (Li et al., 2010), and Ai9 $^{LoxP/LoxP}$ Ai32 $^{LoxP/LoxP}$, *Rosa-tTa* $^{LoxP/LoxP}$.(commercially available from Jax laborites). All mouse strains were maintained on a mixed background (Swiss Webster and C57/ B16). The day of birth is considered P0. Information about the mouse strains including genotyping protocols can be found at http://www.jax.org/ and elsewhere (see above references).

METHOD DETAILS

- **Immunochemistry and imaging**

Embryos, neonate, juvenile and adult mice were perfused inter cardiac with ice cold 4% PFA after being anesthetized on ice (neonates) or using Sleepaway injection. Brains that were processed for immunofluorescence on slides were post-fixed and cryopreserved in 30% sucrose. 16µm coronal sections were obtained using Cryostat (Leica Biosystems) and collected on super-frost coated slides, then allowed to dry and stored at -20˚C until use. For immunofluorescence, cryosections were thawed and allowed to dry for 5-10 min and rinsed in 1x PBS. They were incubated at room temperature in a blocking solution of PBST (PBS-0.1%Tx-100) and 10% normal donkey serum (NDS) for 1hr, followed by incubation with primary antibodies in PBS-T and 1% NDS at 4˚C overnight or 2 days. Samples were then washed 4 times with PBS-T and incubated with fluorescence conjugated secondary Alexa antibodies (Life Technologies) in PBS-T with 1% NDS at room temperature for 1 hr. Slides were incubated for 5min with DAPI, washed 3 times with PBS-T. Then slides were mounted with Fluoromount

G (Southern Biotech) and imaged.

Brains that were processed for free-floating immunofluorescence were first post-fixed in 4% PFA overnight at 4˚C. 50 µm-thickness brain slices were taken on a Leica vibratome and stored in a cryoprotecting solution (40% PBS, 30% glycerol and 30% ethylene glycol) at -20°C. For immunofluorescence, floating sections were blocked for 1hr at RT in normal donkey or goat serum blocking buffer and incubated for 2-3 days at 4°C with primary antibodies in blocking buffer. Sections were washed 4 x 30 min at RT in PBST, incubated overnight at 4°C with secondary antibodies and DAPI in blocking buffer, washed 4 x 30 min at RT in PBST before being mounted on super-frost plus glass slides. Primary antibodies are listed in Key Resource Table.

- **Nova1/2 Localization**

To quantify the Nova localization in SST cINs, mCherry+/SST cIN or KIR2.1+/SST cINs or NaChBac+/SST cIN or Sham+/SST cIN or ECS+/SST cINs or Nova2OE/SST cIN or Nova2OE+KIR2.1/SST cINs were binned into two categories based on the cell compartment Nova1/2 protein was localized to: Cytoplasmic restricted or Nuclear-expressing (comprised of nuclear restricted or whole soma localization). The number of Nuclear-expressing cells was then divided by the number of cytoplasmic restricted cells to obtain a ratio for Nova localization from either mCherry+/SST cIN or KIR2.1+/SST cINs. This was collected from at least three tissue sections from at least 3 animals.

- **Electroconvulsive Shock**

Electroconvulsive stimulation (ECS) was administered to animals with pulses consisting of 1.0 s, 50 Hz, 75 mA stimulus of 0.7 ms delivered using the Ugo Basile ECT unit (Model 57800, as previously described (Guo et al., 2011; Ma et al., 2009). Sham animals were similarly handled the exact same procedure but without the current administration.

- **Confocal imaging and synaptic puncta analysis**

Animals were perfused as described above. Post-fixation incubation prior to cryopreservation was skipped. Cryostat sections (16 µm) were subjected to IHC as described above. Images were taken within the S1 cortex of at least three different sections from at least three different animals per genotype with a Zeiss LSM 800 laser scanning confocal microscope. Scans were performed to obtain 4 optical Z-sections of 0.33 µm each (totaling ~1.2µm max projection) with a 63x/1.4 Oil DIC objective. The same scanning parameters (i.e. pinhole diameter, laser power/offset, speed/averaging) were used for all images. Maximum projections of 4 consecutive 0.33µm stacks were analyzed with ImageJ (NIH) puncta analyzer plugin (Ippolito and Eroglu, 2010) to count the number of individual puncta consisting of pre-synaptic and post-synaptic markers that are close enough together to be considered a putative synaptic puncta. Synaptic puncta density per image was calculated by normalization to total puncta acquired for each individual channel accounted in each image for each condition. Puncta Analyzer plugin is written by Barry Wark, and is available for download (https://github.com/physion/puncta-analyzer). Nova protein intensity was performed as:Cryostat sections of 20 um were immunostained with goat anti-mCherry and human anti-pan Nova (from Darnell Lab). Images were analyzed using Fiji/ImageJ and Nova1/2 protein intensity levels were assessed normalized against area of the cells expressing the AAV.

- **Electrophysiological recordings**

Slice preparation: Acute brain slices (300 µm thick) were prepared from P18-P22 mice. Mice were deeply anesthetized with isofluorane. The brain was removed and placed in ice-cold modified artificial cerebrospinal fluid (ACSF) of the following composition (in mM): 87 NaCl, 26 $NaHCO_3$, 2.5 KCl, 1.25 NaH_2PO_4, 0.5 CaCl, 4 $MgCl_2$, 10 glucose, 75 sucrose saturated with 95% O_2, 5% CO_2 at pH=7.4. Coronal sections were cut using a vibratome (Leica, VT 1200S). Slices were then incubated at 34C for 30 minutes and then stored at room temperature until use.

Recordings: Slices were transferred to the recording chamber of an up-right microscope (Zeiss Axioskop) equipped with IR DIC. Cells were visualized using a 40X IR water immersion objective. Slices were perfused with ACSF of the following composition (in mM): 125 NaCl, 25 $NaHCO_3$, 2.5 KCl, 1.25

NaH2PO4, 2 CaCl2, 1 MgCl2, 20 glucose, saturated with 95% O2, 5% CO2 at pH=7.4 and maintained at a constant temperature (31°C) using a heating chamber. Whole-cell recordings were made from randomly selected tdTomato-positive SST interneurons or tdTomato negative pyramidal cells from layer II-III or layer V of the somatosensory cortex. Recording pipettes were pulled from borosilicate glass capillaries (Harvard Apparatus) and had a resistance of 3-5 MΩ when filled with the appropriate internal solution, as reported below. Recordings were performed using a Multiclamp 700B amplifier (Molecular Devices). The current clamp signals were filtered at 10 KHz and digitized at 40 kHz using a Digidata 1550A and the Clampex 10 program suite (Molecular Devices). Miniature synaptic currents were filtered at 3 kHz and recorded with a sampling rate of 10 kHz. Voltage-clamp recordings where performed at a holding potential of 0mV. Current-clamp recordings were performed at a holding potential of -70 mV. Cells were only accepted for analysis if the initial series resistance was less than 40 MΩ and did not change by more than 20% throughout the recording period. The series resistance was compensated online by at least ~60% in voltage-clamp mode. No correction was made for the junction potential between the pipette and the ACSF.

Passive and active membrane properties were recorded in current clamp mode by applying a series of hyperpolarizing and depolarizing current steps and the analysis was done in Clampfit (Molecular Devices). The cell input resistance was calculated from the peak of the voltage response to a 50 pA hyperpolarizing 1 sec long current step according to Ohm's law. Analysis of the action potential properties was done on the first spike observed during a series of depolarizing steps. Threshold was defined as the voltage at the point when the slope first exceeds a value of 20 V.s-1. Rheobase was defined as the amplitude of the first depolarizing current step at which firing was observed. Analysis of miniature inhibitory events was done using Clampfit's template search.

Pipette solutions: Solution for voltage-clamp recordings from pyramidal cells (in mM): 125 Cs-gluconate, 2 CsCl, 10 HEPES, 1 EGTA, 4 MgATP, 0.3 Na-GTP, 8 Phosphocreatine-Tris, 1 QX-314-Cl and 0.4% biocytin, equilibrated with CsOH at pH=7.3. Solution for current clamp recordings from SST

cINs (in mM): 130 K-Gluconate, 10 KCl, 10 HEPES, 0.2 EGTA, 4 MgATP, 0.3 NaGTP, 5 Phosphocreatine and 0.4% biocytin, equilibrated with KOH CO2 to a pH=7.3.

- ***Nova2* OE/ *Nova2* OE +KIR2.1 Experiment**

SST^{Cre} mice crossed with *Rosa-tTa* $^{LoxP/LoxP}$. were injected at P0/1 with either AAV2/1-DIO-SypGFP at 1:2 dilution with PBS; or AAV2/1-DIO-SynGFP + TRE-Nova2-mCherry (myc tagged) at 1:1:1 dilution with PBS; or AAV2/1-DIO-SynGFP + TRE-Nova2-mCherry (myc tagged) + AAV2/1-DIO-Kir2.1-mCherry at 1:1:1 ratio in the S1 cortex. Mice were perfused at P21, brains harvested, sucrose protected and sectioned on a freezing microtome (Leica) at 20um thickness as described above. Primary antibodies are listed in Key Resource Table.

- **Optogenetic stimulation**

Blue-light (470 nm) was transmitted to the slice from an LED placed under the condenser of an up-right microscope (Olympus BX50). IPSCs were elicited by applying single 1 ms blue-light pulses of varying intensities (max. stimulation intensity ~0.33 mW/mm^2) and directed to layer2/3 or layer5 of the slice in the recording chamber. Light pulses were delivered every 5 seconds. The LED output was driven by a TTL output from the Clampex software of the pCLAMP 9.0 program suite (Molecular Devices).

- **Isolation of cortical interneurons from the developing mouse cerebral cortex**

Cortical interneurons were dissociated from postnatal mouse cortices (P8) as described (Wamsley et al., 2018). We collected at least 3-5 cKO and 3-5 *ctl* brains and maintained overall balanced numbers of females and males within each condition, in order to avoid sex- related gene expression biases. Following dissociation, cortical neurons in suspension were filtered and GFP+ or TdTomato+ fate-mapped interneurons were sorted by fluorescence activated-cell sorting (FACS) on either a Beckman Coulter MoFlo (Cytomation), BD FACSAria II SORP or Sony SY3200. Sorted cINs are collected and lyzed in 200µl TRIzol LS Reagent, then thoroughly mixed and stored at -80˚c until further total RNA extraction.

- **Nucleic acid extraction, RNA amplification, cDNA library preparation and RNA sequencing**

  Total RNAs from sorted SST cINs (P8 mouse S1 cortices for Figure 2, Figure S3, and Figures 5) were extracted using TRIzol LS Reagent and PicoPure columns (if <20K cells were recovered) or PureLink RNA Mini Kit (if >20K cells were recovered), with PureLink DNase for on-column treatment, following the manufacturers' guidelines. RNA quality and quantity were measured with a Picochip using an Agilent Bioanalyzer and only samples with high quality total RNA were used (RIN: 7-10). 20ng of total RNA was used for cDNA synthesis and amplification, using NuGEN Ovation RNA-Seq System V2 kit (NuGEN part # 7102). 100 ng of amplified cDNA were used to make a library using the Ovation Ultralow Library System (NuGEN part # 0330). The samples were mulitplexed and subjected to 50-nucleotide paired-end read rapid with the Illumina HiSeq 2500 sequencer (v4 chemistry), to generate >50 million reads per sample. Library preparation, quantification, pooling, clustering and sequencing was carried out at the NYULMC Genome Technology Center. qRT-PCR (quantitative RT-PCR) was performed using SYBR select master mix (Thermo-Fisher Scientific) on cDNA synthesized using SuperScript II reverse transcriptase and oligo(dT) primers.

List of RT- and qRT-PCR primers:

Primer name	Sequence
Adam22-FAM-fw	CGTCGCCGTCCAGCTCGACCAGGGAATAATTGCCGGCACCAT
Adam22-Rv	GCGAGGTCTCCCATTTTCAC
Anks1b-FAM-Fw	CGTCGCCGTCCAGCTCGACCAGGCTCCCTAGACGTTCCTCAC
Anks1b-FAM-Fw	GGATGATGCTGCCAGTACTG
Sez6-FAM-Fw	CGTCGCCGTCCAGCTCGACCAGCCACCATCCACTTCTCCTGT
Sez6-Rev	GCTCCCTAGACGTTCCTCAC
Dlg3-FAM-Fw	CGTCGCCGTCCAGCTCGACCAGTTCCCTGGGTTAAGTGACGA
Dlg3-Rev	TCATCGTTGACTCGGTCCTT

Syngap1-FAM-Fw	CGTCGCCGTCCAGCTCGACCAGAACATCCAAAGGCAGCCAAG
Syngap1-Rev	GCCGGCTCACATAGAAAAGG
Prkrir-FAM-Fw	CGTCGCCGTCCAGCTCGACCAGGGGTTGAGAATTGTAGGAGAGC
Prkrir--Rev	CTGCTATGCGGGTTGTTCAA
Sorbs2-FAM-Fw	CGTCGCCGTCCAGCTCGACCAGCGATCGGAGCCAAGGAGTAT
Sorbs2-Rev	AGGCTTCTGTCTATGGAGGAC
Nrxn1-FAM-Fw	CGTCGCCGTCCAGCTCGACCAGACACCTGATGATGGGCGAC
Nrxn1-Rev	TGAAGCATCAGTCCGTTCCT
Ezh2-FAM-Fw	CGTCGCCGTCCAGCTCGACCAGTGAGAAGGGACCGGTTTGTT
Ezh2-Rev	GCATTCAGGGTCTTTAACGGG
Triobp-FAM-Fw	CGTCGCCGTCCAGCTCGACCAGACCCTAGCCAATGGACACAG
Triobp-Rev	CTTGAAGTTGAGCAGATCGGG
Itch-FAM-Fw	CGTCGCCGTCCAGCTCGACCAGTGCATTTCACAGTGGCCTTC
Itch-Rev	CCCATGGAATCAAGCTGTGG

- **Bioinformatics**

Downstream computational analysis were performed at the NYULMC Genome Technology Center. All the reads were mapped to the mouse reference genome (mm10) using the STAR aligner (Dobin et al., 2013). Quality control of RNAseq libraries (i.e. the mean read insert sizes and their standard deviations) was calculated using Picard tools (v.1.126) (http://broadinstitute.github.io/picard/). The Read Per Million (RPM) normalized BigWig files were generated using BEDTools (v2.17.0) (Quinlan and Hall, 2010) and bedGraphToBigWig tool (v4). For the SST cIN P8 ECS, approx. 60E6-80E6 reads were aligned per sample; for P8 SST-Nova1, SST-Nova2, SST-dKO, approx. 60E6-70E6 reads were aligned per sample; for P8 SST-cIN wt ECS and SST-Nova-dKO ECS, approx. 60E6-80E6 reads were aligned per sample. The samples processed for downstream analysis were as follows: 9 samples for SST cIN +ECS versus SST cIN ctl at P8 (4/5 samples per condition), 6 samples for *SST-Nova1* removal versus

SST cIN ctl (3 samples per genotype), 6 samples for *SST-Nova2* removal versus SST cIN ctl (3 samples per genotype), 6 samples for *SST-dKO* removal versus SST cIN ctl (3 samples per genotype) and 7 samples for *SST-dKO* removal ECS versus SST cIN ctl ECS (4 control samples, 3 cKO samples).

We used rMATS (v3.0.9) (Shen et al., 2014) to quantify the AS event types (i.e.skipped exons (SE), alternative 3' splice sites (A3SS), alternative 5' splice sites (A5SS), mutually exclusive exons (MXE) and retained introns (RI)). rMATS uses a counts-based model, it detects AS events using splice junction and exon body counts and calculates an exon inclusion level value ψ for each event in each condition. It then determines the differential $|\Delta\psi|$ value across conditions (cut-offs for significance were placed at *FDR*<0.05 and $|\Delta\psi|\geq 0.1$). To compare the level of similarity among the samples and their replicates, we used two methods: classical multidimensional scaling or principal-component analysis and Euclidean distance-based sample clustering. The downstream statistical analyses and generating plots were performed in Rstudio (Version 1.1.456) (http://www.r- project.org/).

To assess the enrichment for the Nova-binding motif in the differentially regulated exons we utilized rMAPS (Park et al., 2016). We utilized the raw output from rMATS analysis (6 RNAseq experiments of SST cINs +ECS vs SST cINs ctl) with significant splicing events cut off at FDR>50%. rMAPS performs position weight analysis to assess the enrichment of RNA binding protein binding motifs in the exonic and flanking intronic regions of up-regulated or down-regulated exons and plots the motif density along with a given pValue in comparison to unregulated exons.

We performed GO analysis using the DAVID online Bioinformatics Resources 6.8 at FDR >0.05 (unless otherwise specified) (Huang et al., 2008) and tested PPI networks by utilizing DAPPLE at 10,000 permutations (Rossin et al., 2011).

- **Validation of SST-cINs AS activity-dependent exons by RT-PCR**

Total RNAs from sorted cINs from wt SST cINs, ECS SST cINs, and ECS SST-dKO were extracted as described above and at least three independent biological replicates were used in each experiment. RT-PCR validation of regulated exons was performed as described before (Han et al., 2014). After

denaturation, samples were run on 10% Novex™ TBE-Urea Gels (ThermoFisher). Gels were directly scanned by ChemiDoc™ Imaging System (Bio-Rad) and quantified by ImageStudio program (Licor).

QUANTIFICATION AND STATISTICAL ANALYSIS

In all figures: *, *p*-value<0.05; **, *p*-value<0.01; ***, *p*-value<0.001; ****, *p*-value<0.0001. Statistical analyses for motif enrichment was performed by rMAPS and differential alternative splicing changes were performed using rMATS. Percentages were compared with repeated t-tests in *GraphPad Prism* or *Rstudio*, and means ± (standard deviation, SD) are represented. As well as, some statistical analyses and generating plots were performed in R environment (v3.1.1) (http://www.r- project.org/).

All values presented in the manuscript are average ± standard error of the mean (SEM). The statistical values for the intrinsic physiology are obtained using one-way ANOVA with Bonferroni correction for multiple comparisons between the different genotypes: Controls, Nova1-cKO, Nova2-cKO and Nova-dKO (*p ≤ 0.05, **p ≤ 0.01, ***p ≤ 0.005). For the Channelrhodopsin output, student's t-test was used to compare Control vs Nova1-cKO, and Control vs Nova2-cKO (*p ≤ 0.05, **p ≤ 0.01, ***p ≤ 0.005).

DATA AND SOFTWARE AVAILABILITY The accession number for the RNA sequencing data reported in this paper is NCBI GEO: [*TBD*].

Figure legends

Figure 1. Neuronal activity affects the synaptic development of SST cINs

A) Schematic of genetic alleles (left) and experimental approach (middle), *SSTCre;Syp-eGFP* pups were injected with a conditional virus; either *AAV2/1-Flex-Kir2.1-P2A-mCherry, AAV2/1-Flex-NaChBac-P2A-mCherry,* or Control *AAV2/1-Flex-mCherry* within the S1 cortex at postnatal day 0 (P0). Schematic of the efferent connectivity of SST+ Martinotti cells (right).

B) Immunostaining (IHC) of *SSTCre;Syp-eGFP* in layer 1 (L1) of S1 cortex at P21 showing Syp-eGFP (green, anti-GFP) and axons (red, anti-RFP) from *control, Kir2.1, or NaChBac* injected SST+ Marintonotti cINs (scale bar 50um).

C) Quantification of SST cIN axonal density within L1 of somatosensory cortex of control, KIR2.1, and NaChBac injected *SST^{cre}* animals (pVal*=0.011, ***=0.0008).

D) Visualization of Syp-eGFP (green, anti-GFP) and Gephyrin+ puncta (blue, anti-Gephyrin) in L1 SST+ cINs (scale bar 20um). Inset shows a higher magnification image of the puncta overap (Red, mCherry axons).

E) Quantification of synaptic puncta (RFP+/GFP+/Gephyrin+ overlap) of control, Kir2.1, and NaChBac expressing SST+ cINs within L1 (pVal**= 0.008, ***=0.0001).

Figure 2. Neuronal activity influences alternative splicing and Nova expression within SST cINs

A) Schematic of experimental approach: Postnatal day 8 (P8) *SST^{Cre};RCE^{eGFP}* or *SSTCre;Ai9* pups were to electroconvulsive shock (ECS) (left). Following 2-3 hours the S1 cortex was isolated and SST+ cINs were FACS purified (middle). SST+ cINs were then prepared for RNAseq to assess changes in alternative splicing. Splicing changes are divided into the major alternative structural motifs: single exon, SE, retained intron, RI, mutually exclusive exons, MXE, alternative 5' splice site, A5, alternative 3' splice site, A3 (right).

B) Histogram of the magnitude of activity-dependent splicing changes within SST+ cINs subjected to ECS compared to sham SST+ cINs (FDR <0.5, fold <0.1>), depicting 139 differential spliced SE (82 SE included, 57 SE excluded), 66 differential spliced RI (53 RI included, 13 RI excluded), 55 differential spliced MXE (26 included, 29 excluded), 13 differential spliced A5 (12 included, 1 excluded), 39 differential spliced A3 (16 included, 23 excluded).

C) Sashimi plot illustrating *Nxrn1* exon 10 exclusion in activity-induced SST cINs in green (bottom) compared to sham SST cINs in grey (top). Reads per kilobase of transcripts (RPKM) gives the count of the number of transcripts for a specfic isoform.

D) Histogram of the average motif enrichment score of known activity-regulated splicing factors KHDRBS1 (Sam68), KHDRBS2 (SLM2), Rbfox1 and Nova1/2 (right). Green dots represents -log10 adjusted p value (right Y-axis) for motif enrichment scores, only significant enrichment shown.

E) Bubble dot plot of gene ontology (GO) most significant terms for the genes subjected to activity-dependent alternative splicing within SST+ cINs (false discovery rate (FDR)<0.05), x-axis is the enrichment of the activity-dependent AS genes in the GO catagory (# of genes in GO category from SST transcriptome/ # of genes activity-dependent AS in category). Color of dot indicates magnitude of significance (-log10 transform FDR, none shown above FDR <0.05) and size corresponds to number of genes in catagory. F) Protein-protein interaction (PPI) network formed from 312 activity-depdendent spliced genes in SST cINs with Disease Association Protein-Protein Link Evaluator (DAPPLE) (Rossin et al., 2011) and performed over 10,000 permutations (pVal<0.00009). Green shading- post-synaptic gene network, pink shading- pre-synaptic gene network.

Figure 3. Neuronal activity during cortical development influences the expression and localization of Nova proteins in SST cINs.

A) Relative gene expression of *Nova1* (orange) and *Nova2* (pink), normalized to house-keeping gene Peptidyl prolyl isomerase A (*PPIA)* using qPCR from Lhx6-eGFP sorted cINs at Postnatal age (P) P2, P8 and P15.

B) Fold change of the relative expression of *Nova1* and *Nova2* between cINs and excitatory neurons (cExt) showing an enrichment of Nova expression in cINs at early developmental ages.

C) Model of experimental approach: Acute activity induction via electrical stimulation (ECS) followed by qPCR 1.5 hrs post stimulation (HRPS), Western and IHC 2.5HRPS at P8.

D) Relative expression of *Nova1* and *Nova2* genes (using qPCR) of ECS induced SST cINs relative to controls (**pVal=0.002, *Nova1*; **pVal=0.005, *Nova2).*

E) Upper panel, western blot showing Nova1 and Nova2 protein expression in control (lanes 2 and 3) versus ECS induced SST cINs (lanes 4 and 5). Lower panel, same western blot showing expression of b-actin across lanes.

F) Quantification of the western blot data. Nova1 and Nova2 protein expression relative to b-actin in control versus ECS induced SST cINs (*pVal=0.038, Nova1; *pVal=0.022, Nova2).

G) Representative scoring criteria for Nova1/2 localization within SST cINs: IHC of Nova1/2 (blue, anti-Nova1/2) in selective SST+ cINS exemplifying the Nova1/2 expression in: cytoplasm only (top), in both cytoplasm and nucleus (middle), and nucleus only (bottom).

H) Representative images of Nova1/2 expression in SST cINs under normal versus ECS

I) Quantification of the ratio of nuclear to cytoplasmic localization of Nova1/2 in SST+ cINs of control animals (grey) and ECS animals (black) **pVal= 0.001.

J) Schematic of the constitutive activity manipulation via injection of DIO:AAVs (*AAV2/1-Flex-mCherry, AAV2/1-Flex-NaChBac-P2A-mCherry,* and *AAV2/1Flex-Kir2.1- P2A-mCherry*) at P0 followed by IHC at P21.

K) Left, Quantification of the ratio of nuclear to cytoplasmic localization of Nova1/2 in SST+ cINs of control *AAV2/1-Flex-mCherry* (grey) versus *AAV2/1-Flex-NaChBac-P2A-mCherry.* Right, Quantification of the ratio of nuclear to cytoplasmic localization of Nova1/2 in SST+ cINs of control (grey) *AAV-2/1-Flex-mCherry* (grey) versus *AAV2/1-Flex-Kir2.1- P2A-mCherry* (blue) injected animals. ***pVal=0.0004, NachBac; ***pVal=0.0001, KIR2.1

L) Quantification of the number of Nova1/2-expressing SST+ cINs of control *AAV2/1-Flex-mCherry* (grey) and *AAV2/1-Flex-Kir2.1- P2A-mCherry* (blue) injected animals. ***pVal= 0.0001

M) Representative images of Nova1/2 expression, Top: control SST cIN (injected with mCherry), Bottom: KIR2.1+ SSt cIN at P21.

N) Quantification of Nova1/2 protein pixel intensity (normalized to area) from ctl SST cINs (grey) and KIR2.1+ SST cINs (blue).

Figure 4. *SST-Nova1 and SST-Nova2* mutants have impaired afferent and efferent connectivity.

A) SST+ cINs efferent structure: IHC of anti-RFP (red), anti-VGAT (green), and anti-Gephyrin (blue) to label the SST+ cIN axonal synaptic puncta (RFP+/VGAT+/Gephyrin+ puncta, white) in L1 S1 cortex of *SST-ctl, SST-Nova1,* and *SST-Nova2* mutant animals.

B) Quantification of the density of SST+ cIN efferent synaptic puncta (RFP+/VGAT+/Gephyrin+) in L1 S1 cortex of *SST-ctl, SST-Nova1* and *SST-Nova2* mutant animals. **pVal=0.003, *SST-Nova1*; ***pVal<0.0001, *SST-Nova2*

C) Schematic of channelrhodopsin (ChR2) experimental approach: SST-Cre control, SST-Nova1 or SST-Nova2 mutant mice were crossed with the Ai32 reporter line that expresses ChR2 in a Cre dependent manner. Blue light was delivered through the objective to record inhibtory response (IPSC) in neighboring excitatory neuron (grey).

D) Top: Example trace of inhibitory output from control SST+ cIN within S1 of SST-ctl (grey trace), and *SST-Nova1* mutant *(*orange trace*)*. Bottom: control SST+ cIN within S1 (grey trace), *SST-Nova2 (*pink trace) animals. Right: Quantification of the peak IPSC amplitudes recorded in excitatory neurons following SST stimulation. **pVal=0.0037, *SST-Nova1*; **pVal=0.0021, *SST-Nova2.*

E) SST+ afferents: IHC of representative SST+ cIN dendrite of anti-RFP (red), anti-VGLUT1 (green), and anti-Homer1c (blue) to label excitatory synaptic puncta overlapping with SST+ cINs dendrites (RFP+/VGLUT1+/Homer1c+ puncta, white) in S1 cortex of *SST-ctl, SST-Nova1 and SST-Nova2* mutant animals.

F) Quantification of the density of excitatory afferent synapses onto SST+ cINs within L2/3 and L5/6 of S1 cortex of *SST-ctl, SST-Nova1 and SST-Nova2* mutant animals. *pVal=0.028, *SST-Nova1*; *pVal=0.012, *SST-Nova2*.

G) Schematic of experimental approach recording mini-excitatory postsynaptic potentials (mEPSCs) in SST+ cINs in the S1 cortex (red).

H) Quantification of mEPSCs frequencies from SST+ cIN *Ctl,SST-Nova1 and SST-Nova2* mutant animals.

Figure 5. Nova RNA binding proteins control activity dependent AS in SST cINS during development

A) Schematic of experimental approach: Control and *SST-dKO* P8 animals were subjected to ECS then the S1 cortex was isolated to FACS purify SST+ cINs followed by RNAseq and splicing analysis.

B) Magnitude of activity-dependent splicing changes within *SST-dKO* subjected to ECS compared to Ctr *SST-wt* cINs subjected to ECS (FDR <0.5, fold <0.1>), depicting 166 differential spliced SE (106 SE included, 60 SE excluded), 72 differential spliced RI (51 RI included, 21 RI excluded), 70 differential spliced MXE (37 included, 33 excluded), 9 differential spliced A5 (7 included, 2 excluded), 29 differential spliced A3 (9 included, 20 excluded).

C) Example RT-PCR validation of alternative splicing (AS) events of activity- and Nova1/2- dependent alternative exon usage within the gene *Syngap1* (left), Gel image of RT-PCR product from the amplification of exon13 to exon 15 within *SST-ctl* cINs (Ctl) (left), ECS-treated Ctl (middle), and ECS-treated *SST-dKO* (right).

D) Quantification of RT-PCR AS events of *Syngap1.* **pVal=0.0001 Ctl vs Ctl+ECS; **pVal=0.004 Ctl+ECS vs *SST-dKO*+ECS.

E) Bubble dot plot of the most significant GO terms for the genes undergoing Nova1/2 activity-dependent AS within SST+ cINs (all shown GO terms FDR<0.05) (Same graph parameters as Figure2E).

F) Schematic of a SST+ cIN pre-synaptic inhibitory axonal puncta (top right) and a SST+ cIN excitatory post-synaptic density (middle left) overlaid on top of the significant DAPPLE generated PPI diect network from the 346 genes undergoing Nova1/2-dependent activity induced AS (***pVal=0.00009, 10000 permutations).

Figure 6. *Nova2* overexpression within SST cINs augments axonal growth and synaptic formation in an activity dependent manner.

A) Experimental model: Schematic of genetic alleles (left) crossed to generate mice for injection of *AAV2/1-Flex-Syp-eGFP* with *AAV2/1-TRE-Nova2-mCherry, or AAV2/1-Flex-Syp-eGFP, AAV2/1-TRE-Nova2-mCherry* and *AAV2/1-Flex-KIR2.1* at P0 followed by IHC at P21.

B) IHC of SST+ cINs axons labeled by Syp-eGFP (Anti-GFP) in control, C) Nova2-OE, and D) Nova2-OE+KIR2.1 injected S1 cortex.

E) Quantification of axonal density of control (grey), Nova2-OE (pink), and Nova2-OE+KIR2.1 (blue)

injected SST+ cINs pVal=*≤ 0.05, **≤ 0.01, ***≤ 0.005

F) Representative images of SST+ cIN axonal efferents within L1 of S1 cortex labeled by Syp-eGFP (anti-GFP, green) and gephryn (anti-gephryn, blue) in Control, G) Nova2OE, and H) Nova2OE+KIR2.1.

I) Quantification of L1 SST+ cIN efferent synaptic puncta via the juxapositon of Syp-eGFP and Gephryn in control (grey), Nova2OE (pink), and Nova2OE +KIR2.1 (blue).

J) Representative images of IHC against mCherry (anti-RFP, red), and Nova1/2 (anti-Nova1/2, blue) in two SST-Nova2OE cells and K) in two SST-Nova2OE+KIR2.1 cells. Top is merge (red/blue) and botton is Nova1/2 (blue) alone.

L) Quantification of the Ratio of Nova1/2 localization within the nucleus to cytoplasm from Nova2OE SSt cINs (pink) and Nova2OE+KIR2.1 (blue). pVal=*≤ 0.05, **≤ 0.01, ***≤ 0.005.

M) Model of experimental findings: center is a cartoon wildtype SST cIN depicting normal expression of Nova1/2 with the soma (red) whereas, on the left, the conditional loss of *Nova1, Nova2,* or the expression of KIR2.1 alone or dual overexpression of Nova2 and KIR2.1 results in the reduction in Nova expression and restricts Nova localization to the cytoplasm (In the case of cKO animals the protein is lost completely). This effect is accompanied by a reduction in the connectivity of SST cINs. To the contrary, Expression of NaChBac and/or overexpression of Nova2 alone results in expression of Nova throughout the cell and nucleus and is accompanied by an increase in the axonal and synaptic density of SST cINs.

References

Adler, A., Zhao, R., Shin, M.E., Yasuda, R., Gan, W.-B., 2019. Somatostatin-Expressing Interneurons Enable and Maintain Learning-Dependent Sequential Activation of Pyramidal Neurons. Neuron 1–23. doi:10.1016/j.neuron.2019.01.036

Allene, C., Cattani, A., Ackman, J.B., Bonifazi, P., Aniksztejn, L., Ben-Ari, Y., Cossart, R., 2008. Sequential Generation of Two Distinct Synapse-Driven Network Patterns in Developing Neocortex. Journal of Neuroscience 28, 12851–12863. doi:10.1523/JNEUROSCI.3733-08.2008

Allene, C., Cossart, R., 2010. Early NMDA receptor-driven waves of activity in the developing neocortex: physiological or pathological network oscillations? The Journal of Physiology 588, 83–91. doi:10.1113/jphysiol.2009.178798

Basaldella, E., Takeoka, A., Sigrist, M., Arber, S., 2015. Multisensory Signaling Shapes Vestibulo-Motor Circuit Specificity. Cell 163, 301–312. doi:10.1016/j.cell.2015.09.023

Bortone, D., Polleux, F., 2009. KCC2 Expression Promotes the Termination of Cortical Interneuron Migration in a Voltage-Sensitive Calcium-Dependent Manner. Neuron 62, 53–71. doi:10.1016/j.neuron.2009.01.034

Cossart, R., 2011. The maturation of cortical interneuron diversity: how multiple developmental journeys shape the emergence of proper network function. Curr. Opin. Neurobiol. 21, 160–168. doi:10.1016/j.conb.2010.10.003

De Marco García, N.V., Karayannis, T., Fishell, G., 2011. Neuronal activity is required for the development of specific cortical interneuron subtypes. Nature 472, 351–355. doi:10.1038/nature09865

Denaxa, M., Neves, G., Rabinowitz, A., Kemlo, S., Liodis, P., Burrone, J., Pachnis, V., 2018. Modulation of Apoptosis Controls Inhibitory Interneuron Number in the Cortex. Cell Reports 22, 1710–1721. doi:10.1016/j.celrep.2018.01.064

Dredge, B.K., Darnell, R.B., 2003. Nova regulates GABA(A) receptor gamma2 alternative splicing via a distal downstream UCAU-rich intronic splicing enhancer. Molecular and Cellular Biology 23, 4687–4700. doi:10.1128/mcb.23.13.4687-4700.2003

Eom, T., Zhang, C., Wang, H., Lay, K., Fak, J., Noebels, J.L., Darnell, R.B., 2013. NOVA-dependent regulation of cryptic NMD exons controls synaptic protein levels after seizure. Elife 2, 5752–29. doi:10.7554/eLife.00178

Favuzzi, E., Deogracias, R., Marques-Smith, A., Maeso, P., Jezequel, J., Exposito-Alonso, D., Balia, M., Kroon, T., Hinojosa, A.J., F Maraver, E., Rico, B., 2019. Distinct molecular programs regulate synapse specificity in cortical inhibitory circuits. Science 363, 413–417. doi:10.1126/science.aau8977

Fishell, G, Rudy, B., 2011. Mechanisms of Inhibition within the Telencephalon: “Where the Wild Things Are.” Annu. Rev. Neurosci. 34, 535–567. doi:10.1146/annurev-neuro-061010-113717

Furlanis, E., Scheiffele, P., 2018. Regulation of Neuronal Differentiation, Function, and Plasticity by Alternative Splicing. Annu. Rev. Cell Dev. Biol. 34, 451–469. doi:10.1146/annurev-cellbio-100617-062826

Furlanis, E., Traunmüller, L., Fucile, G., Scheiffele, P., 2019. Landscape of ribosome-engaged transcript isoforms reveals extensive neuronal-cell-class- specific alternative splicing programs. Nature Neuroscience 1–15. doi:10.1038/s41593-019-0465-5

Garaschuk, O., Linn, J., Eilers, J., Konnerth, A., 2000. Large-scale oscillatory calcium waves in the immature cortex. Nature Neuroscience 3, 452–459. doi:10.1038/74823

Gong, S., Zheng, C., Doughty, M.L., Losos, K., Didkovsky, N., Schambra, U.B., Nowak, N.J., Joyner, A., Leblanc, G., Hatten, M.E., Heintz, N., 2003. A gene expression atlas of the central nervous system based on bacterial artificial chromosomes. Nature Publishing Group 425, 917–925. doi:10.1038/nature02033

Guo, J.U., Ma, D.K., Mo, H., Ball, M.P., Jang, M.-H., Bonaguidi, M.A., Balazer, J.A., Eaves, H.L., Xie, B., Ford, E., Zhang, K., Ming, G.-L., Gao, Y., Song, H., 2011. Neuronal activity modifies the DNA methylation landscape in the adult brain. Nature Neuroscience 14, 1345–1351. doi:10.1038/nn.2900

Iijima, T., Wu, K., Witte, H., Hanno-Iijima, Y., Glatter, T., Richard, S., Scheiffele, P., 2011a. SAM68 regulates neuronal activity-dependent alternative splicing of neurexin-1. Cell 147, 1601–1614. doi:10.1016/j.cell.2011.11.028

Iijima, T., Wu, K., Witte, H., Hanno-Iijima, Y., Glatter, T., Richard, S., Scheiffele, P., 2011b. SAM68 regulates neuronal activity-dependent alternative splicing of neurexin-1. Cell 147, 1601–1614. doi:10.1016/j.cell.2011.11.028

Ippolito, D.M., Eroglu, C., 2010. Quantifying synapses: an immunocytochemistry-based assay to quantify synapse number. J Vis Exp. doi:10.3791/2270

Kapfer, C., Glickfeld, L.L., Atallah, B.V., Scanziani, M., 2007. Supralinear increase of recurrent inhibition during sparse activity in the somatosensory cortex. Nature Neuroscience 10, 743–753. doi:10.1038/nn1909

Karayannis, T., De Marco García, N.V., Fishell, G.J., 2012. Functional adaptation of cortical interneurons to attenuated activity is subtype-specific. Front Neural Circuits 6, 66. doi:10.3389/fncir.2012.00066

Kepecs, A., Fishell, G, 2014. Interneuron cell types are fit to function. Nature 505, 318–326. doi:10.1038/nature12983

Le Magueresse, C., Monyer, H., 2013. GABAergic Interneurons Shape the Functional Maturation of the Cortex. Neuron 77, 388–405. doi:10.1016/j.neuron.2013.01.011

Lee, J.-A., Xing, Y., Nguyen, D., Xie, J., Lee, C.J., Black, D.L., 2007. Depolarization and CaM Kinase IV Modulate NMDA Receptor Splicing through Two Essential RNA Elements. PLoS Biol 5, e40–14. doi:10.1371/journal.pbio.0050040

Lee, J.A., Tang, Z.Z., Black, D.L., 2009. An inducible change in Fox-1/A2BP1 splicing modulates the alternative splicing of downstream neuronal target exons. Genes & Development 23, 2284–2293. doi:10.1101/gad.1837009

Li, L., Tasic, B., Micheva, K.D., Ivanov, V.M., Spletter, M.L., Smith, S.J., Luo, L., 2010. Visualizing the Distribution of Synapses from Individual Neurons in the Mouse Brain. PLoS ONE 5, e11503–13. doi:10.1371/journal.pone.0011503

Licatalosi, D.D., Mele, A., Fak, J.J., Ule, J., Kayikci, M., Chi, S.W., Clark, T.A., Schweitzer, A.C., Blume, J.E., Wang, X., Darnell, J.C., Darnell, R.B., 2008. HITS-CLIP yields genome-wide insights into brain alternative RNA processing. Nature 456, 464–469. doi:10.1038/nature07488

Lim, L., Mi, D., Llorca, A., Marín, O., 2018. Development and Functional Diversification of Cortical Interneurons. Neuron 100, 294–313. doi:10.1016/j.neuron.2018.10.009

Lin, C.-W., Sim, S., Ainsworth, A., Okada, M., Kelsch, W., Lois, C., 2010. Genetically increased cell-intrinsic excitability enhances neuronal integration into adult brain circuits. Neuron 65, 32–39. doi:10.1016/j.neuron.2009.12.001

Liu, Z., Wang, L., Welch, J.D., Ma, H., Zhou, Y., Vaseghi, H.R., Yu, S., Wall, J.B., Alimohamadi, S., Zheng, M., Yin, C., Shen, W., Prins, J.F., Liu, J., Qian, L., 2017. Single-cell transcriptomics reconstructs fate conversion from fibroblast to cardiomyocyte. Nature Publishing Group 551, 100–104. doi:10.1038/nature24454

Ma, D.K., Jang, M.H., Guo, J.U., Kitabatake, Y., Chang, M.L., Pow-anpongkul, N., Flavell, R.A., Lu, B., Ming, G.L., Song, H., 2009. Neuronal Activity-Induced Gadd45b Promotes Epigenetic DNA Demethylation and Adult Neurogenesis. Science 323, 1074–1077. doi:10.1126/science.1166859

Marín, O., 2016. Developmental timing and critical windows for the treatment of psychiatric disorders. Nature Publishing Group 22, 1229–1238. doi:10.1038/nm.4225

Mauger, O., Lemoine, F., Scheiffele, P., 2016. Targeted Intron Retention and Excision for Rapid Gene Regulation in Response to Neuronal Activity. Neuron 92, 1266–1278. doi:10.1016/j.neuron.2016.11.032

Minlebaev, M., Colonnese, M., Tsintsadze, T., Sirota, A., Khazipov, R., 2011. Early γ oscillations synchronize developing thalamus and cortex. Science 334, 226–229. doi:10.1126/science.1210574

Muñoz, W., Tremblay, R., Levenstein, D., Rudy, B., 2017. Layer-specific modulation of neocortical dendritic inhibition during active wakefulness. Science 355, 954–959. doi:10.1126/science.aag2599

Nigro, M.J., Hashikawa-Yamasaki, Y., Rudy, B., 2018. Diversity and Connectivity of Layer 5 Somatostatin-Expressing Interneurons in the Mouse Barrel Cortex. Journal of Neuroscience 38, 1622–1633. doi:10.1523/JNEUROSCI.2415-17.2017

Park, J.W., Jung, S., Rouchka, E.C., Tseng, Y.-T., Xing, Y., 2016. rMAPS: RNA map analysis and plotting server for alternative exon regulation. Nucleic Acids Res 44, W333–W338. doi:10.1093/nar/gkw410

Priya, R., Paredes, M.F., Karayannis, T., Yusuf, N., Liu, X., Jaglin, X., Graef, I., Alvarez-Buylla, A., Fishell, G., 2018. Activity Regulates Cell Death within Cortical Interneurons through a Calcineurin-Dependent Mechanism. Cell Reports 22, 1695–1709. doi:10.1016/j.celrep.2018.01.007

Quesnel-Vallières, M., Dargaei, Z., Irimia, M., Gonatopoulos-Pournatzis, T., Ip, J.Y., Wu, M., Sterne-Weiler, T., Nakagawa, S., Woodin, M.A., Blencowe, B.J., Cordes, S.P., 2016. Misregulation of an Activity-Dependent Splicing Network as a Common Mechanism Underlying Autism Spectrum Disorders. Molecular Cell 64, 1023–1034. doi:10.1016/j.molcel.2016.11.033

Racca, C., Gardiol, A., Eom, T., Ule, J., Triller, A., Darnell, R.B., 2010. The Neuronal Splicing Factor Nova Co-Localizes with Target RNAs in the Dendrite. Front Neural Circuits 4, 5. doi:10.3389/neuro.04.005.2010

Rossin, E.J., Lage, K., Raychaudhuri, S., Xavier, R.J., Tatar, D., Benita, Y., International Inflammatory Bowel Disease Genetics Constortium, Cotsapas, C., Daly, M.J., 2011. Proteins Encoded in Genomic Regions Associated with Immune-Mediated Disease Physically Interact and Suggest Underlying Biology. PLoS Genet 7, e1001273–13. doi:10.1371/journal.pgen.1001273

Saito, Y., Miranda-Rottmann, S., Ruggiu, M., Park, C.Y., Fak, J.J., Zhong, R., Duncan, J.S., Fabella, B.A., Junge, H.J., Chen, Z., Araya, R., Fritzsch, B., Hudspeth, A.J., Darnell, R.B., 2016. NOVA2-mediated RNA regulation is required for axonal pathfinding during development. Elife 5, 487. doi:10.7554/eLife.14371

Saito, Y., Yuan, Y., Zucker-Scharff, I., Fak, J.J., Jereb, S., Tajima, Y., Licatalosi, D.D., Darnell, R.B., 2019. Differential NOVA2-Mediated Splicing in Excitatory and Inhibitory Neurons Regulates Cortical Development and Cerebellar Function. Neuron 1–20. doi:10.1016/j.neuron.2018.12.019

Silberberg, G., Markram, H., 2007. Disynaptic Inhibition between Neocortical Pyramidal Cells Mediated by Martinotti Cells. Neuron 53, 735–746. doi:10.1016/j.neuron.2007.02.012

Sousa, V.H., Miyoshi, G., Hjerling Leffler, J., Karayannis, T., Fishell, G., 2009. Characterization of Nkx6-2-Derived Neocortical Interneuron Lineages. Cerebral Cortex 19, i1–i10. doi:10.1093/cercor/bhp038

Taniguchi, H., He, M., Wu, P., Kim, S., Paik, R., Sugino, K., Kvitsani, D., Fu, Y., Lu, J., Lin, Y., Miyoshi, G., Shima, Y., Fishell, G., Nelson, S.B., Huang, Z.J., 2011. A Resource of Cre Driver Lines for Genetic Targeting of GABAergic Neurons in Cerebral Cortex. Neuron 71, 995–1013. doi:10.1016/j.neuron.2011.07.026

Tremblay, R., Lee, S., Rudy, B., 2016. GABAergic Interneurons in the Neocortex: From Cellular Properties to Circuits. Neuron 91, 260–292. doi:10.1016/j.neuron.2016.06.033

Ule, J., Jensen, K., Mele, A., Darnell, R.B., 2005. CLIP: A method for identifying protein–RNA interaction sites in living cells. Methods 37, 376–386. doi:10.1016/j.ymeth.2005.07.018

Ule, J., Stefani, G., Mele, A., Ruggiu, M., Wang, X., Taneri, B., Gaasterland, T., Blencowe, B.J., Darnell, R.B., 2006. An RNA map predicting Nova-dependent splicing regulation. Nature 444, 580–586. doi:10.1038/nature05304

Vuong, C.K., Black, D.L., Zheng, S., 2016. The neurogenetics of alternative splicing. Nat Rev Neurosci 17, 265–281. doi:10.1038/nrn.2016.27

Vuong, C.K., Wei, W., Lee, J.-A., Lin, C.-H., Damianov, A., la Torre Ubieta, de, L., Halabi, R., Otis, K.O., Martin, K.C., O'Dell, T.J., Black, D.L., 2018. Rbfox1 Regulates Synaptic Transmission through the Inhibitory Neuron-Specific vSNARE Vamp1. Neuron 98, 127–141.e7. doi:10.1016/j.neuron.2018.03.008

Wamsley, B., Fishell, G, 2017. Genetic and activity-dependent mechanisms underlying interneuron diversity. Nature Publishing Group 18, 299–309. doi:10.1038/nrn.2017.30

Wamsley, B., Jaglin, X.H., Favuzzi, E., Quattrocolo, G., Nigro, M.J., Yusuf, N., Khodadadi-Jamayran, A., Rudy, B., Fishell, G., 2018. Rbfox1 Mediates Cell-type-Specific Splicing in Cortical Interneurons. Neuron 100, 846–859.e7. doi:10.1016/j.neuron.2018.09.026

Xie, J., Black, D.L., 2001. A CaMK IV responsive RNA element mediates depolarization-induced alternative splicing of ion channels. Nature 410, 936–939. doi:10.1038/35073593

Yang, J.-W., An, S., Sun, J.-J., Reyes-Puerta, V., Kindler, J., Berger, T., Kilb, W., Luhmann, H.J., 2012. Thalamic Network Oscillations Synchronize Ontogenetic Columns in the Newborn Rat Barrel Cortex. Cerebral Cortex 23, 1299–1316. doi:10.1093/cercor/bhs103

Yang, J.W., Hanganu-Opatz, I.L., Sun, J.J., Luhmann, H.J., 2009. Three Patterns of Oscillatory Activity Differentially Synchronize Developing Neocortical Networks In Vivo. Journal of Neuroscience 29, 9011–9025. doi:10.1523/JNEUROSCI.5646-08.2009

Yang, Y., Park, J.W., Bebee, T.W., Warzecha, C.C., Guo, Y., Shang, X., Xing, Y., Carstens, R.P., 2016. Determination of a Comprehensive Alternative Splicing Regulatory Network and Combinatorial Regulation by Key Factors during the Epithelial-to-Mesenchymal Transition. Molecular and Cellular Biology 36, 1704–1719. doi:10.1128/MCB.00019-16

Yano, M., Hayakawa-Yano, Y., Mele, A., Darnell, R.B., 2010. Nova2 Regulates Neuronal Migration through an RNA Switch in Disabled-1 Signaling. Neuron 66, 848–858. doi:10.1016/j.neuron.2010.05.007

Yu, C.R., Power, J., Barnea, G., O'Donnell, S., Brown, H.E.V., Osborne, J., Axel, R., Gogos, J.A., 2004. Spontaneous neural activity is required for the establishment and maintenance of the olfactory sensory map. Neuron 42, 553–566. doi:10.1016/s0896-6273(04)00224-7

Yuan, Y., Xie, S., Darnell, J.C., Darnell, A.J., Saito, Y., Phatnani, H., Murphy, E.A., Zhang, C., Maniatis, T., Darnell, R.B., 2018a. Cell type-specific CLIP reveals that NOVA regulates cytoskeleton interactions in motoneurons 1–19. doi:10.1186/s13059-018-1493-2

Yuan, Y., Xie, S., Darnell, J.C., Darnell, A.J., Saito, Y., Phatnani, H., Murphy, E.A., Zhang, C., Maniatis, T., Darnell, R.B., 2018b. Cell type-specific CLIP reveals that NOVA regulates cytoskeleton interactions in motoneurons 1–19. doi:10.1186/s13059-018-1493-2

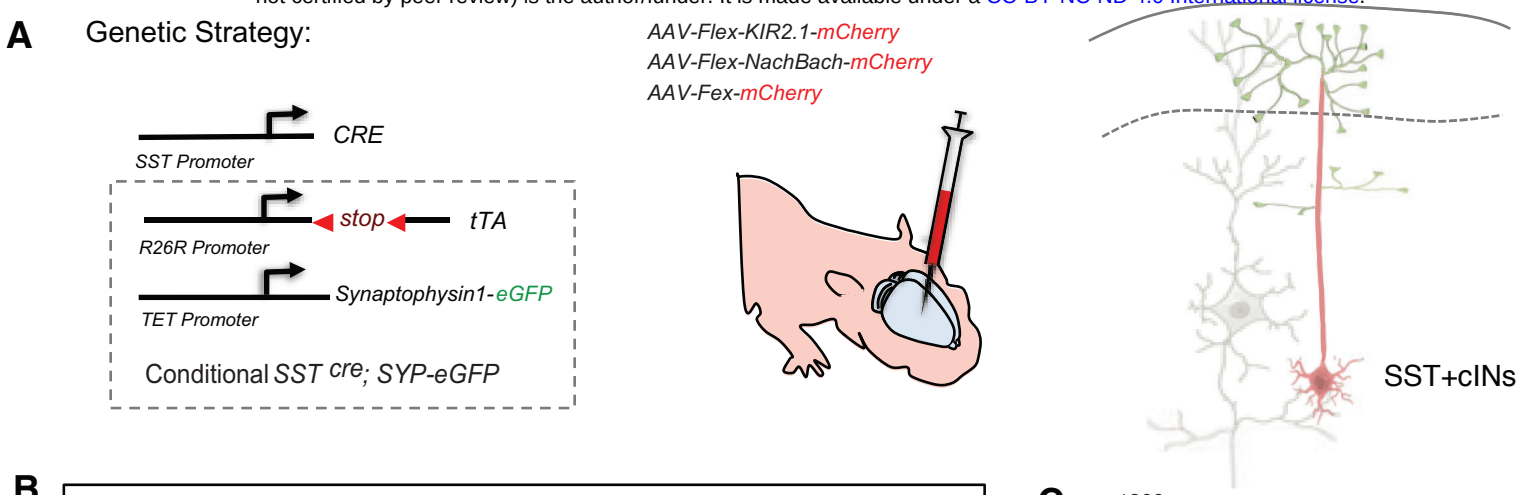

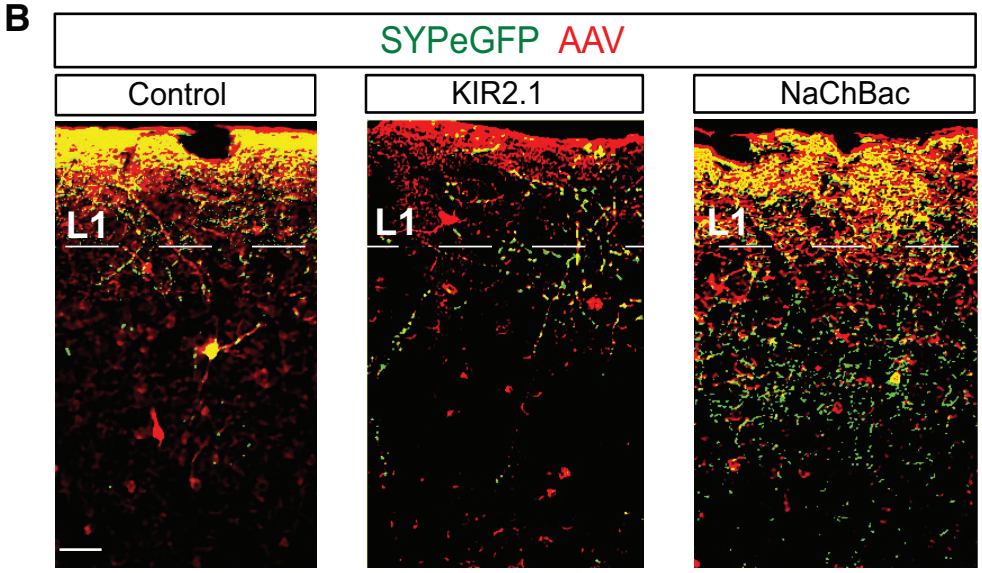

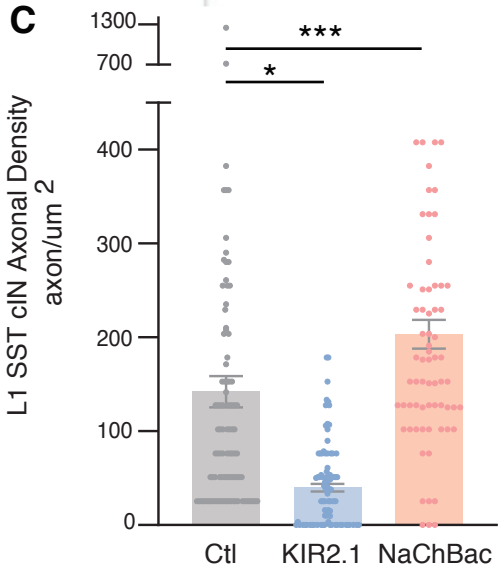

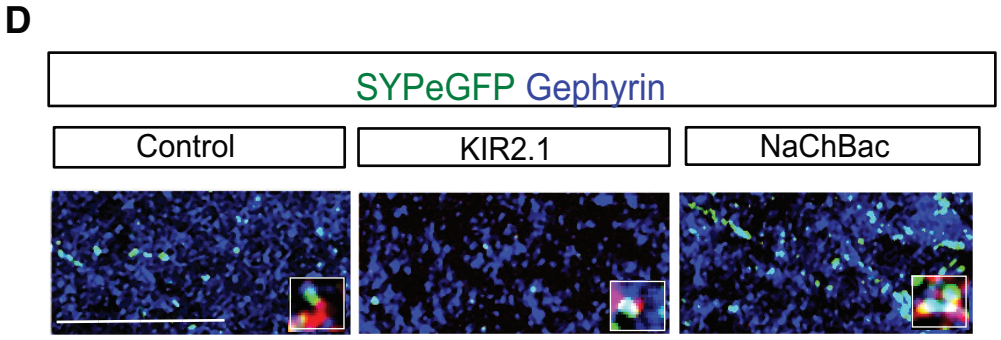

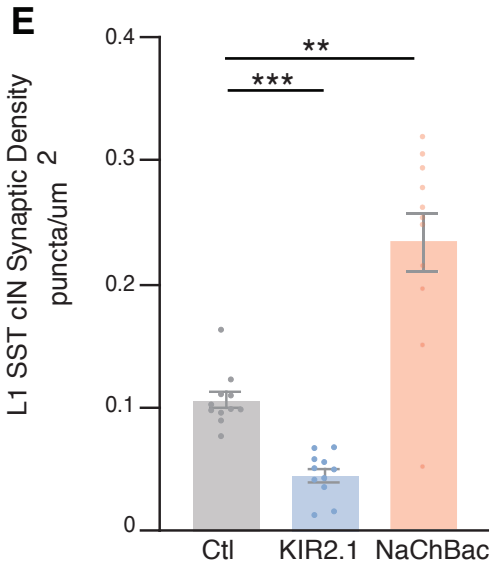

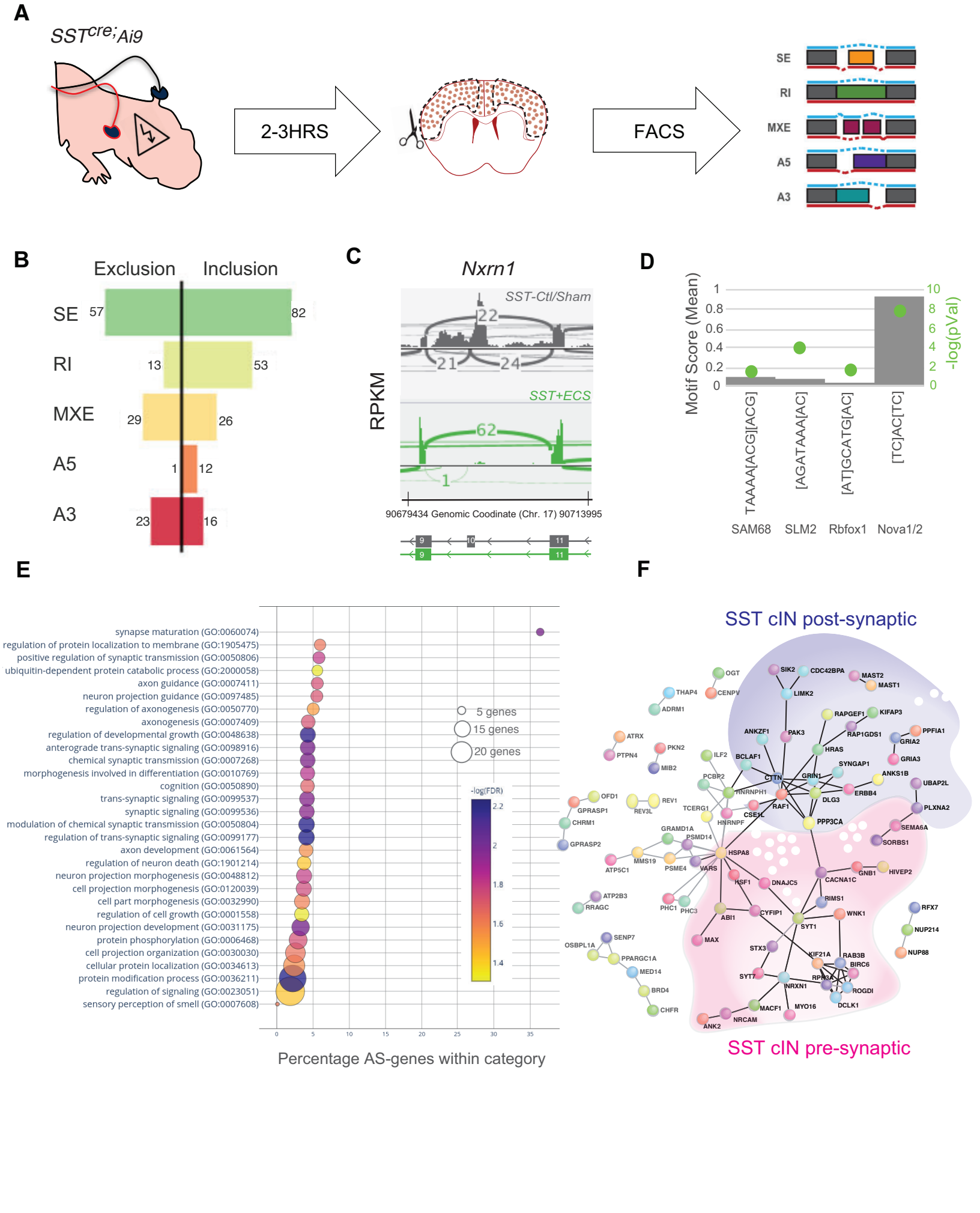

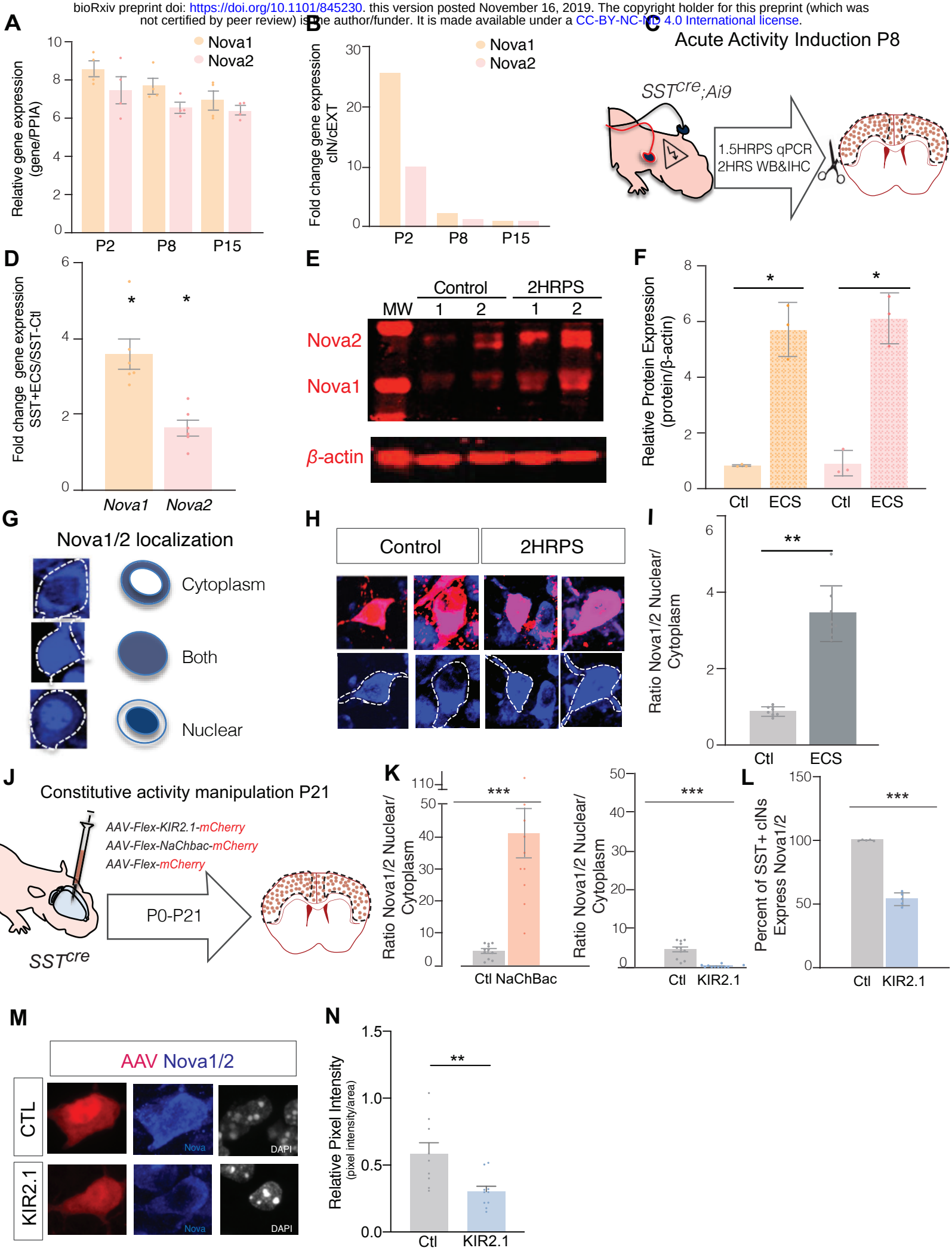

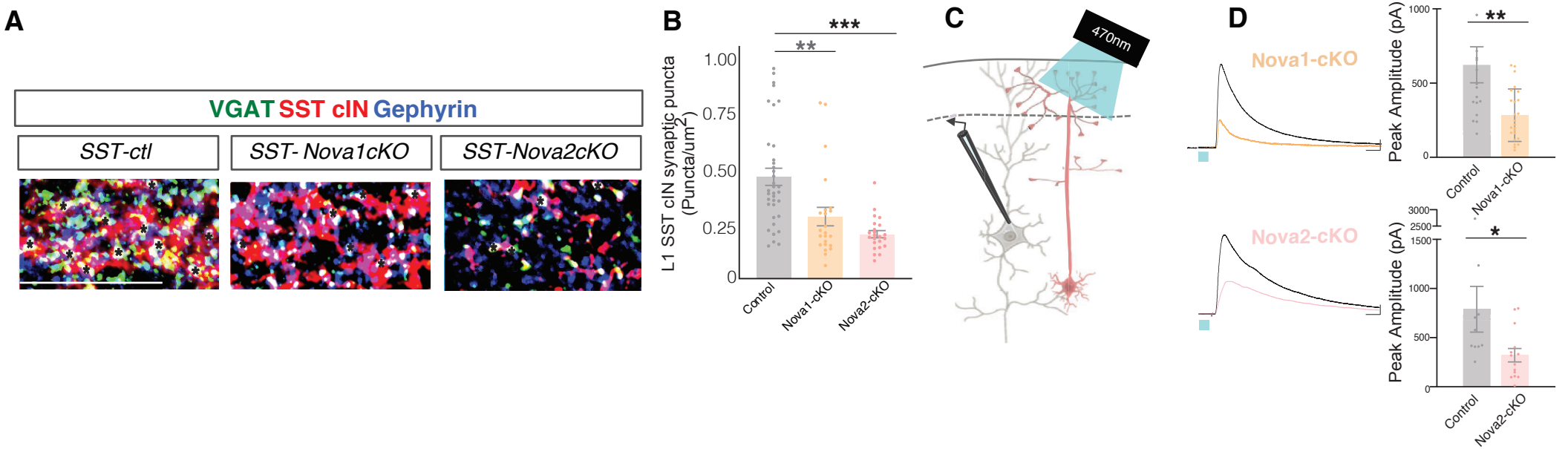
A
VGAT SST cIN Gephyrin
SST-ctl
SST- Nova1cKO
SST-Nova2cKO
B
L1 SST cIN synaptic puncta (Puncta/um2)
1.00
0.75
0.50
0.25
0
***
**
Control
Nova1-cKO
Nova2-cKO
C
470nm
D
Nova1-cKO
Nova2-cKO
Peak Amplitude (pA)
2000
1000
500
0
**
Control
Nova1-cKO
3000
2500
1500
1000
500
0
*
Control
Nova2-cKO

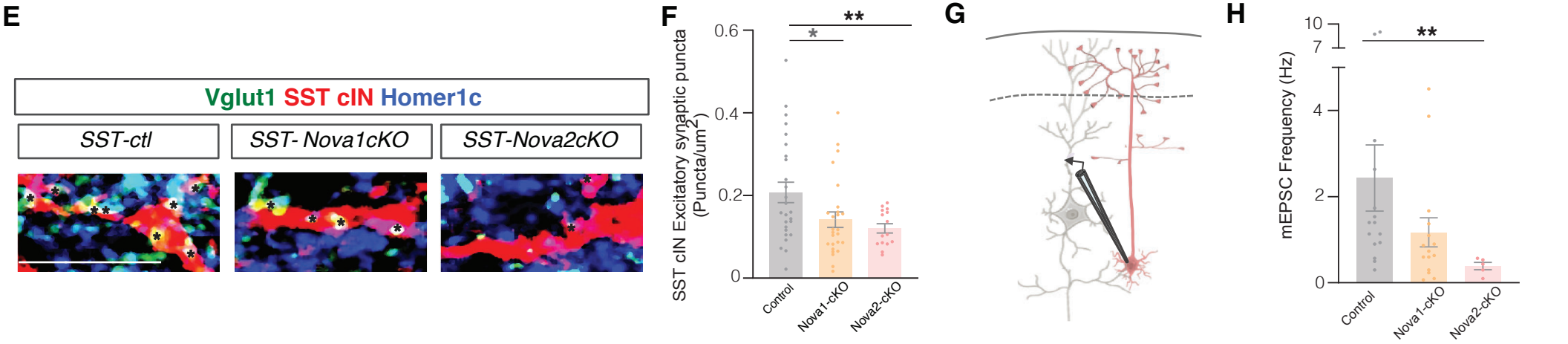
E
Vglut1 SST cIN Homer1c
SST-ctl
SST- Nova1cKO
SST-Nova2cKO
F
SST cIN Excitatory synaptic puncta (Puncta/um2)
0.6
0.4
0.2
0
**
*
Control
Nova1-cKO
Nova2-cKO
G
H
mEPSC Frequency (Hz)
10
7
4
2
0
**
Control
Nova1-cKO
Nova2-cKO